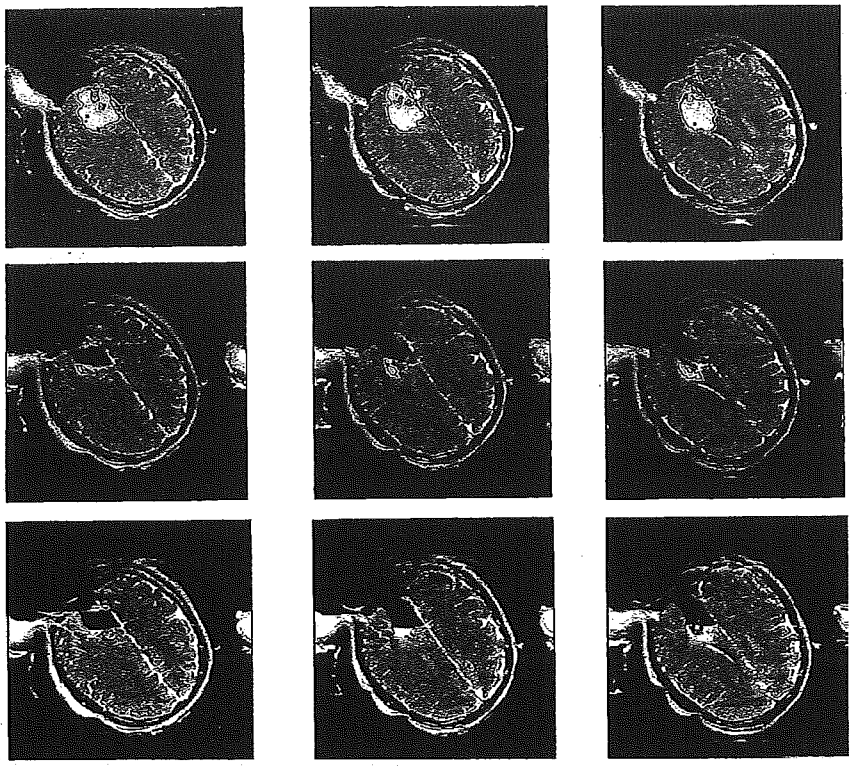

**Figure 1.** Results of intraoperative tumor segmentation in case 7 performed using T2-weighted magnetic resonance imaging (MRI) (repetition time (TR): 1000 milliseconds; echo time (TE): 140 milliseconds; number of excitations (NEX): 1; matrix: 256 × 256; field of view: 230 mm × 230 mm; slice thickness: 1.5 mm; slice gap 3 mm). Images were obtained after dura opening (top row), initial tumor resection (middle row), and total resection of glioma (bottom row). Residual tumor of 1.9 mL, or 5.4% of the total tumor volume (35.1 mL) remained unresected. It was removed in the second half of the operation as is shown in T2-weighted MRI in the bottom row.

### Validation

Two sets of analysis were performed to validate the effectiveness and accuracy of the FC-based segmentation in intraoperative MRI-guided surgery.

The first set of analysis was an unbiased comparison of the results of an actual tumor segmentation performed by the expert neurosurgeons who actually performed the cases and those obtained by the automatic FC-based segmentation. The segmentation results by the expert neurosurgeon were set as gold standard. The goodness of the fit between a gold standard and the results of the automatic segmentation was determined by using an established measure of segmentation accuracy, the dice similarity coefficient (18) and percent match.

The second set of analysis was a detailed examination of intensity profiles obtained around the tumor lesion to determine whether the FC method could be used to enhance the tumor tissue and deemphasize the non–tumor tissue in the fuzzy scene.

## RESULTS

### Postoperative Image Analysis

In these patients, a hyperintense lesion was observed in T2 MR images and a hypointense signal was observed in T1 MR images. Edema was observed in T2 MR images in four cases (#3, #9, #10, and #11). The volume of the tumor in the first set of images ranged from 10.1 to 206.7 mL. A comparison of the results of manual segmentation with those of the automatic FC-based segmentation gave an average dice similarity coefficient of 0.80 (Table 2). The average match was 76%, ranging from 63% (#2) to 84% (#6). In seven of eight studies, the manual segmentation gave a larger volume than the automatic segmentation.

### Clinical Feasibility Study

In all seven patients who underwent intraoperative segmentation and volume measurement, the FC-based segmentation enhanced the residual tumor, which is

**Table 2**
**Accuracy Validation Study**

| Case no. | True positive (mL) (percent match [%]) | False positive (mL) | Dice similarity | Tumor volume | |
|---|---|---|---|---|---|
| | | | | Manual (mL) | Automatic (mL) |
| 1 | 54.6 (83) | 17.2 | 0.79 | 66.2 | 71.8 |
| 2 | 6.4 (63) | 0.8 | 0.74 | 10.1 | 7.2 |
| 3 | 147.4 (71) | 32.1 | 0.76 | 206.7 | 179.5 |
| 4 | 97.4 (80) | 2.7 | 0.88 | 122.3 | 100.1 |
| 5 | 84.7 (73) | 16.2 | 0.78 | 115.4 | 100.9 |
| 6 | 14.4 (84) | 1.1 | 0.88 | 17.1 | 15.5 |
| 7 | 29.0 (76) | 6.1 | 0.79 | 38.2 | 35.1 |
| 8 | 42.5 (81) | 3.8 | 0.86 | 52.4 | 46.3 |
| Average | (76) | | 0.80 | $r^2 = 0.99$ | |

intraoperative MR images was used continuously throughout the surgery.

The intraoperative MRI was T2 axial imaging (two-dimensional fast spin-echo; repetition time (TR): 1000 millisecond; echo time (TE): 140 milliseconds, number of excitations (NEX): 1; matrix: 256 × 256; field of view: 230 mm × 230 mm; slice thickness: 1.5 mm; slice gap: 3 mm) standard in routine clinical practice at the institution. No contrast agent was administered in any of the cases.

The first eight cases were examined with a goal of postoperative validation to assess the accuracy of automatic segmentation compared with that of manual segmentation. The last seven cases (ie, cases 6–12) involved actual intraoperative image segmentation in the operative theater.

## Intraoperative Segmentation and Volume Measurement

We used the fuzzy connectedness (FC) method to perform intraoperative brain tumor segmentation. The FC method (11) was first proposed for application to medical image segmentation (12), followed by reports on tumor segmentation in MRI (13–15). We chose the FC method for the segmentation of brain tumor in intraoperative MRIs for the following reasons. First, the method has proven to be accurate and reliable in brain tumor segmentation using MRI (13). Second, the role of the operator with the FC method is limited to the selection of representative points in the tumor, which means that the method is suitable for intraoperative settings. Starting from the selected seed point in the tissue of interest (ie, tumor), the method calculates the affinity of the neighboring voxels by using two criteria: how close the voxels are spatially and how similar they are in image intensity. The algorithm automatically computes a fuzzy scene (a map of fuzzy connectivity) in 3D from gray-scale images.

The FC algorithm without competition paradigm requires two parameters: a seed point and a threshold for the fuzzy scene. An operator sets the seed point in the region of the tumor by clicking one pixel on the monitor. The operator also limits the region to be analyzed by enclosing the whole tumor in a rectangle and inputting the numbers of the first and last slices. This procedure shortens the processing time. A threshold is then set in the precomputed fuzzy scene.

FC-based software was developed and implemented on a Linux PC (CPU: Pentium 4, 2.53 GHz; RAM: 1024 MB) using the 3D Slicer software program (Brigham and Women's Hospital and Massachusetts Institute of Technology; Boston, MA). The 3D Slicer is a surgical simulation and navigation software program that displays multimodality images three- and two-dimensionally (16,17). The 3D Slicer was used in this study to transfer intraoperative images from the scanner and perform tumor segmentation followed by volume measurement. The Linux PC was set up next to the scanner console in our interventional MRI suite and was used for segmentation, volume measurement, and surgical guidance.

After the segmentation, the total number of the voxels classified to tumor tissue is counted. Multiplying pixel area and slice gap size to this total number of voxels yields the volume of the tumor.

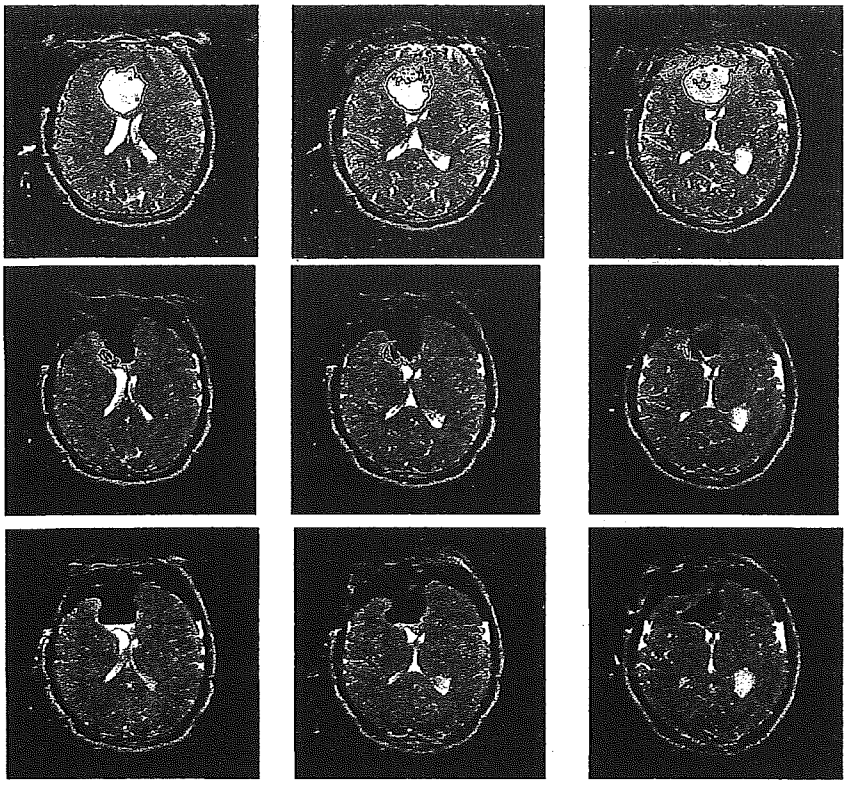

**Figure 2.** Intraoperative tumor segmentation in T2-weighted magnetic resonance imaging after dura opening (top row), initial tumor resection (middle row), and total resection of glioma (bottom row) in case 8. The images in each row are shown in the inferior-to-superior order. Note that the fuzzy connectedness–based segmentation clearly delineates the tumor and cyst boundary in the first scan (top row). In the second scan (middle row), 2.6 mL, or 6.2%, of the tumor (42.1 mL before the resection) was delineated by segmentation. No tumor was observed in the images obtained before dura closure (bottom row).

difficult to observe directly in MRI or hard to correctly identify by simple thresholding. The tumor volume measurement also facilitated decision-making during tumor resection.

In case 7, segmentation and augmented visualization of residual tumor was particularly important after the first step of tumor resection when the physician was engaged in surgical control, and careful study of images was difficult. After removing most of the tumor (33.2 mL, or 94.6%), a residual tumor of 1.9 mL was delineated by using the proposed segmentation method. In a second step of tumor resection, the tumor was completely removed (Fig. 1).

In case 8, as illustrated in Fig. 2, a frontal tumor of 43.7 mL was removed in the first step of the surgery. However, after T2-weighted MRI scanning, 2.6 mL, or 5.7%, of residual tumor was delineated by segmentation. We then continued the tumor removal toward the nonresected tissue area and achieved total resection.

An illustrative fuzzy scene from case 8 strongly enhanced the site of the tumor over the ventricles; the tumor tissue is classified to tumor by simple thresholding in original T2 images (Fig 3). However, in the fuzzy scene, the intensity of the tumor site was more pronounced than in the neighboring ventricles. The border between the tumor site and the surrounding nontumor tissue in the fuzzy scene also changed more steeply than in the original gray-scale images.

In all the cases, the scanning time was approximately 5 minutes for 100 slices, which was followed by image transfer to the computing workstation. The image processing took approximately 30 seconds. The computing time was short enough not to disturb the operation.

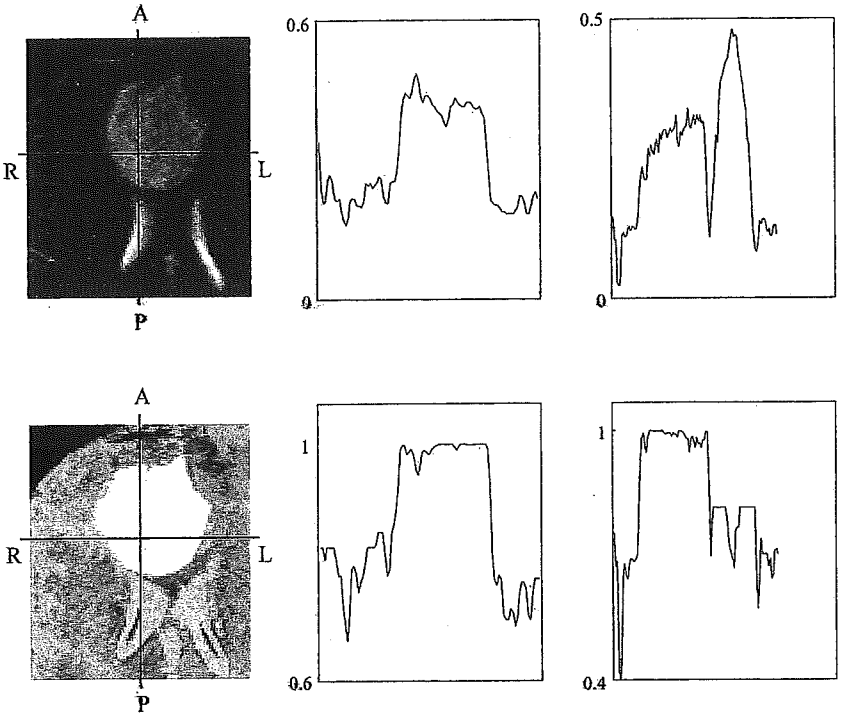


**Figure 3.** Intensity profiles obtained from original gray-scale T2-weighted magnetic resonance imaging (MRI) (top) and fuzzy science (bottom) after fuzzy connectivity-based segmentation. Compared with the intensity profiles obtained along the right-left line (top middle) and the anterior-posterior line (top right) in gray-scale MRI, the profiles along the right-left line (bottom middle) and the anteroposterior line (bottom right) in fuzzy scene have more distinct tumor delineation.

## DISCUSSION

The preliminary results of the clinical feasibility and validation studies have lead us to believe that FC-based segmentation using intraoperative MRI can be used to accurately measure residual tumor and facilitates gross-total resection of glioma. We believe that this method provides a useful clinical addition to glioma surgery and treatment options aimed at minimizing the recurrence of glioma.

An average dice similarity coefficient of 0.80 agrees with the results obtained in other studies (18) of brain segmentation in MRI. We found that FC-based segmentation is not as effective as manual segmentation when the tumor is close to a surrounding nontumor object/tissue or when the border around the tumor is blurred because of intervention. This poor image quality may have negatively affected the FC-based segmentation in clinical settings. This might also be the cause why average match of 76% obtained in our study was slightly less than that reported previously (19), in which brain tumor was segmented by k-nearest neighbor rule and a semisupervised fuzzy c-means method. A possible solution to overcome these image quality issue is to perform MRI intensity standardization and inhomogeneity correction as preprocessing steps. The former particularly can help improving consistency of performance from one study to another.

We employed the FC method without competition paradigm as opposed to competition paradigm. The FC method without competition can detect only one object at a time and requires thresholding of the connectedness map. The FC method with competition, or relative FC, may be suitable for intraoperative MRI segmentation because it does not require thresholding. Relative FC may also help resolving the issues of incorrect segmentation on fuzzy boundary and incorrect inclusion of nearby nontumor objects into tumor tissue class.

A paucity of material is available on segmentation of a tumor in intraoperative MR images (20). To the authors' best knowledge, this is the first attempt to segment a tumor in series of intraoperative MRI studies.

Therefore, the engineering significance of our study lies in the applicability of the developed tool in real surgical setting in which limited user-software interaction and both speed and robustness of tumor segmentation in poor MRI quality are crucial. This study was also clinically significant because it provided evidence that such tool enables quantitative measurement of the volume of tumor resection and facilitates the resection of tumors.

In conclusion, the FC tumor segmentation method can be used for intraoperative tumor segmentation and volume measurement in MRI-guided glioma surgery using 0.3-T open magnets. The results lead us to conjecture that the method can provide unbiased resection rate of tumor for strategic surgical decision-making, and ultimately minimize the amount of residual tumor.

## ACKNOWLEDGMENTS

We are grateful to Drs. Takeyoshi Dohi and Tomokatsu Hori for technical and clinical assistance.

## REFERENCES

1. Berger MS, Deliganis AV, Dobbins J, et al. The effect of extent of resection on recurrence in patients with low-grade cerebral hemisphere gliomas. Cancer 1994; 74:1784–1791.
2. Philippon JH, Clemenceau SH, Fauchon FH, et al. Supratentorial low-grade astrocytomas in adults. Neurosurgery 1993; 32:554–559.
3. Hammoud MA, Ligon BL, ElSouki R, et al. Use of intraoperative ultrasound for localizing tumors and determining the extent of resection: a comparative study with magnetic resonance imaging. J Neurosurg 1996; 84:737–741.
4. Chacko AG, Kumar NK, Chacko G, et al. Intraoperative ultrasound in determining the extent of resection of parenchymal brain tumours—a comparative study with computed tomography and histopathology. Acta Neurochir (Wien) 2003; 145:743–748; discussion 748.
5. Unsgaard G, Ommedal S, Muller T, et al. Neuronavigation by intraoperative three-dimensional ultrasound: initial experience during brain tumor resection. Neurosurgery 2002; 50:804–812; discussion 812.
6. Lindseth F, Lango T, Bang J, et al. Accuracy evaluation of a 3D ultrasound-based neuronavigation system. Comput Aided Surg 2002; 7:197–222.
7. Jodicke A, Accomazzi V, Reiss I, et al. Virtual endoscopy of the cerebral ventricles based on 3-D ultrasonography. Ultrasound Med Biol 2003; 29:339–345.
8. Broggi G, Ferroli P, Franzini A, et al. CT-guided neurosurgery: preliminary experience. Acta Neurochir Suppl 2003; 85:101–104.
9. Black PM, Moriarty T, Alexander E, et al. Development and implementation of intraoperative magnetic resonance imaging and its neurosurgical applications. Neurosurgery 1997; 41:831–842.
10. Schneider JP, Schulz T, Schmidt F, et al. Gross-total surgery of supratentorial low-grade gliomas under intraoperative MR guidance. AJNR Am J Neuroradiol 2001; 22:89–98.
11. Udupa JK, Saha PK, Fuzzy connectedness and image segmentation. Proc IEEE 2003; 91:1649–1669.
12. Udupa JK, Samarasekera S. Fuzzy connectedness and object definition: theory, algorithms, and applications in image segmentation. Graph Models Image Process 1996; 58:246–261.
13. Moonis G, Liu J, Udupa JK, et al. Estimation of tumor volume with fuzzy-connectedness segmentation of MR images. AJNR Am J Neuroradiol 2002; 23:356–363.
14. Udupa JK, Wei L, Samarasekera S, et al. Multiple sclerosis lesion quantification using fuzzy-connectedness principles. IEEE Trans Med Imaging 1997; 16:598–609.
15. Liu J, Udupa JK, Odhnera D, et al. System for upper airway segmentation and measurement with MR imaging and fuzzy connectedness. Acad Radiol 2003; 10:13–24.
16. Hata N, Jinzaki M, Kacher D, et al. MR imaging-guided prostate biopsy with surgical navigation software: device validation and feasibility. Radiology 2001; 220:263–268.
17. Gering DT, Nabavi A, Kikinis R, et al. An integrated visualization system for surgical planning and guidance using image fusion and an open MR. J Magn Reson Imaging 2001; 13:967–975.
18. Zijdenbos AP, Dawant BM, Margolin RA, et al. Morphometric analysis of white-matter lesions in MR-images—method and validation. IEEE Trans Med Imaging 1994; 13:716–724.
19. Velthuizen RP, Clarke LP, Phuphanich S, et al. Unsupervised measurement of brain tumor volume on MR images. J Magn Reson Imaging 1995; 5:594–605.
20. Warfield SK, Nabavi A, Butz T, et al. Intraoperative segmentation and nonrigid registration for image guided therapy. In Delp SL, DiGioia AM, Jaramaz B, eds: Medical image computing and computer-assisted intervention. Berlin, Germany: Miccai 2000; 176–185.

## Spectroscopy and Navigation

To The Editor: With great interest we read the article of Stadlbauer, et al. (Stadlbauer A, Moser E, Gruber S, et al: Integration of biochemical images of a tumor into frameless stereotaxy achieved using a magnetic resonance imaging/magnetic resonance spectroscopy hybrid data set. *J Neurosurg 101*:287–294, August, 2004), about integration of the spectroscopic data into frameless stereotaxy system for intraoperative neuronavigation during removal of cerebral gliomas.

*Abstract*

*Object.* It is often difficult to delineate the extent of invasion of high- and low-grade gliomas into normal brain tissue by using conventional $T_1$- and $T_2$-weighted magnetic resonance (MR) imaging. Knowledge of the relationship between the tumor infiltration zone and normal brain, however, is one of the prerequisites for performing as radical a tumor resection as possible. Proton MR spectroscopy allows noninvasive measurements of the concentrations and spatial distributions of brain metabolites and, therefore, may provide biochemical information in vivo, that is useful in distinguishing pathological from normal areas of the brain.

The authors have developed a method to use the properties of MR spectroscopy to investigate intraoperatively pathological changes in the spatial distribution of choline (Cho)-containing compounds, total creatine, and *N*-acetyl-aspartate (NAA) in brain tumors with the aid of frameless stereotaxy.

*Methods.* Maps of the Cho/NAA ratio were calculated and automatic segmentation of the tumors was performed. Spectroscopic images of the segmented tumor were matched to an anatomical three-dimensional (3D) MR imaging set by applying a fully automated mutual-information algorithm. The resulting 3D MR image can be used subsequently for neurosurgical planning, transfer to a frameless stereotactic system, and display in the navigation microscope during surgery leading to $^1$H-MR spectroscopy-guided navigation.

*Conclusions.* This method may allow better intraoperative identification of tumor border zones based on metabolic changes due to tumor infiltration.

The authors believe that additional biochemical information provided by proton MR spectroscopy could be helpful for more aggressive tumor resection. The general criticisms of this concept from the biological point of view were given in the editorial by Kelly.[3] We wish to make additional comments, considering the intrinsic limitations of MR spectroscopy by itself, which may be an obstacle to the authors' goals.

First, proton MR spectroscopy is very sensitive but not a specific diagnostic modality. Elevation of MR spectroscopy–detected levels of Cho-containing compounds may be caused by both cell membrane synthesis and degradation and therefore may be observed not only in brain tumors, but also in gliosis, inflammation, and early necrosis.[4,5] A decrease in NAA accompanies any brain dysfunction and can be identified in the areas of peritumoral edema.[1,2,7] The degree of representation of the tumor within MR spectroscopy voxels may significantly influence the data obtained.[6] Postprocessing analysis of the spectroscopic data is also important. For example, in the referenced article the standard deviations of mean frequencies used for calculations of the peak intensities for Cho, Cr, and NAA (3.14, 2.94, and 1.82 ppm, respectively) seems to be too great. Therefore, identification of the borders of gliomas based on the data of Cho/NAA ratio alone is highly susceptible for both false-negative and false-positive results.

Second, the magnetic field strength of commonly used clinical MR imagers (1.5 tesla) usually limits the size of MR spectroscopy voxel to 1 cm$^3$. Even if the authors of the referenced article were able to reduce it to 0.25 cm$^3$, it still seems too large for use as a guide for tumor resection. It should be noted that any errors will be further augmented by use of the preoperative data in the intraoperative neuronavigation, which do not take into account the degree of brain shift. Moreover, the authors used sequential acquisitions for MR spectroscopy and MR imaging data with further coregistration. Any changes to the patient's head position between investigations will lead to mislocalization errors. In fact, at present we use MR spectroscopy–guided frame-based stereotactic biopsy of parenchymal brain tumors. Both MR imaging and multivoxel MR spectroscopy are performed after fixation of a stereotactic frame with the use of a localizer, which permits further precise cross-registration of the data within SurgiPlan (Elekta Instruments AB, Elekta, Sweden)

In conclusion, proton MR spectroscopy is an invaluable diagnostic modality in neurooncology, which can be extremely helpful for differential diagnosis of the brain tumor, noninvasive evaluation of its proliferative activity, grade and type, and monitoring of the therapeutic response. Magnetic resonance spectroscopy–guided stereotactic biopsy at least theoretically permits more accurate target selection. In our opinion, however, incorporation of the preoperative MR imaging data into intraoperative neuronavigation system with a goal to attain a higher degree of glioma resection seems technically interesting but impractical due to several biological and technical limitations, which are particularly attributable to the method itself, at least in its present state of development.

Mikhail F. Chernov, M.D.
Yoshihiro Muragaki, M.D.
Taku Ochiai, M.D.
Takashi Maruyama, M.D.
Masahiro Izawa, M.D.
Motohiro Hayashi, M.D.
Yuko Ono, M.D.
Osami Kubo, M.D.
Tomokatsu Hori, M.D.
Neurological Institute
Tokyo Women's Medical University
Tokyo, Japan

### References

1. Chernov M, Kubo O, Ono Y, Hayashi M, Izawa M, Abe K, et al: Proton MRS study of the neuronal function in the peritumoral brain tissue. **Brain Tumor Pathol 20 (Suppl):155, 2003 (Abstract)**
2. Kamada K, Houkin K, Iwasaki Y, Abe H, Kashiwaba T: In vivo proton magnetic resonance spectroscopy for metabolic changes of human brain edema. **Neurol Med Chir 34:676–681, 1994**
3. Kelly PJ: Technology in the resection of gliomas and the definition of madness. **J Neurosurg 101:284–286, 2004**
4. Kwock L, Smith JK, Castillo M, Ewend MG, Cush S, Hensing T, et al: Clinical applications of proton MR spectroscopy in oncology. **Technol Cancer Res Treat 1:17–28, 2002**
5. Lee PL, Gonzalez RG: Magnetic resonance spectroscopy of brain tumors. **Curr Opin Oncol 12:199–204, 2000**
6. Sijens PE, van Dijk P, Oudkerk M: Correlation between choline level and Gd-DTPA enhancement in patients with brain metastases of mammary carcinoma. **Magn Reson Med 32:549–555, 1994**

7. Sijens PE, Oudkerk M: $^1$H chemical shift imaging characterization of human brain tumor and edema. **Eur Radiol 12:2056–2061, 2002**

RESPONSE: We thank the colleagues for their thoughtful comments regarding our experience with neuronavigation and MR spectroscopy.

We fully agree that inaccuracies due to brain shift and technical limitations of the navigation system are of concern when using this method. A correlation between the areas of peritumoral abnormalities depicted by MR spectroscopy and pathological findings will be published shortly.[1] Calculation of metabolic maps by integrating the peak area of a metabolite of interest for each voxel is a common method of visualizing these changes.[2,5] The full-width-at-half-maximum (FWHM) of the peaks of Cho, Cr, and NAA ranges from 10 to 14 Hz (for NAA). In our opinion, however, for full determination of the individual metabolite signals it is necessary to choose a wider interval than the FWHM for calculation to determine the whole peak area. The integration interval for calculation the intensities of the peak signals in our publication was at most 0.4 ppm for NAA (0.2 ppm for Cho and Cr), which is equivalent to less than 26 Hz (13 Hz) at 1.5 tesla. Depending on the line shape, a more narrow frequency range for integration can lead to a severe underestimation of metabolite levels.

In a recently published article from our group[4] we were able to demonstrate higher sensitivity of $^1$H-MR spectroscopy with a spatial resolution of approximately 0.5 cm$^3$ (nominal voxel size actually 0.25 cm$^3$), that is, if the effect of the 50% Hamming filter applied is taken into consideration, in combination with a segmentation algorithm compared to a routine tumor MR imaging strategy. For a full review of the application of various novel imaging tools in neurosurgery, and in particular MR spectroscopic imaging,[3] the reader may be interested in an upcoming special issue in *Neurosurgery Clinics of North America on MRI*.

ANDREAS STADLBAUER, PH.D.
OLIVER GANSLANDT, M.D.
EWALD MOSER, PH.D.
Neurochirurgische Klinik der Universität Erlangen-Nürnberg
Erlangen, Germany
Medical University of Vienna
Vienna, Austria

### References

1. Ganslandt O, Stadlbauer A, Fahlbusch R, Kamada K, Buslei R, Blumcke I, Moser E, Nimsky C: Proton magnetic resonance spectroscopic imaging integrated into image guided surgery: correlation to standard magnetic resonance imaging and tumor cell density. **Neurosurgery** (In press)
2. Luyten PR, Marien AJ, Heindel W, van Gerwen PH, Herholz K, den hollander JA, et al: Metabolic imaging of patients with intracranial tumors: H-1 MR spectroscopic imaging and PET. **Radiology 176:791–799, 1990**
3. Stadlbauer A, Gruber S, Mlynarik V, Gatterbauer B, Roessler K, Moser E: Proton MR spectroscopic imaging in brain tumor diagnosis. **Neurosurgery Clinics of North America on MRI 16: 101–114, 2005**
4. Stadlbauer A, Moser E, Gruber S, Buslei R, Nimsky C, Fahlbusch R, et al: Improved delineation of brain tumors: an automated method for segmentation based on pathologic changes of (1)H-MRSI metabolites in gliomas. **Neuroimage 23:454–461, 2004**
5. van Der Veen JWC, Weinberger DR, Tedeschi G, Frank JA, Duyn JH: Proton MR spectroscopic imaging without water suppression. **Radiology 217:296–300, 2000**

## Brachial Plexus Injury

To THE EDITOR: We read with great interest the article by Belzberg, et al. (Belzberg AJ, Dorsi MJ, Storm PB, et al: Surgical repair of brachial plexus injury: a multinational survey of experienced peripheral nerve surgeons. *J Neurosurg 101*:365–376, September, 2004).

*Abstract*

*Object.* Brachial plexus injuries (BPIs) are often devastating events that lead to upper-extremity paralysis, rendering the limb a painful extraneous appendage. Fortunately, there are several nerve repair techniques that provide restoration of some function. Although there is general agreement in the medical community concerning which patients may benefit from surgical intervention, the actual repair technique for a given lesion is less clear. The authors sought to identify and better define areas of agreement and disagreement among experienced peripheral nerve surgeons as to the management of BPIs.

*Methods.* The authors developed a detailed survey in two parts: one part addressing general issues related to BPI and the other presenting four clinical cases. The survey was mailed to 126 experienced peripheral nerve physicians and 49 (39%) participated in the study. The respondents represent 22 different countries and multiple surgical subspecialties. They performed a mean of 33 brachial plexus reconstructions annually. Areas of significant disagreement included the timing and indications for surgical intervention in birth-related palsy, treatment of neuroma-in-continuity, the best transfers to achieve elbow flexion and shoulder abduction, the use of intra- or extraplexal donors for motor neurotization, and the use of distal or proximal coaptation during nerve transfer.

*Conclusions.* Experienced peripheral nerve surgeons disagree in important ways as to the management of BPI. The decisions made by the various treating physicians underscore the many areas of disagreement regarding the treatment of BPI, including the diagnostic approach to defining the injury, timing of and indications for surgical intervention in birth-related palsy, the treatment of neuroma-in-continuity, the choice of nerve transfers to achieve elbow flexion and shoulder abduction, the use of intra- or extraplexal donors for neurotization, and the use of distal or proximal coaptation during nerve transfer.

The authors developed a detailed questionnaire regarding how experienced peripheral nerve surgeons would treat hypothetical cases of BPI. Interestingly, these authors observed a great variability among these surgeons regarding management of BPI.

In the same issue Kline[2] commented on this article and outlined some significant aspects of treatment of BPI. He described some generally accepted observations regarding the management of BPI. One of these observations was that in his experience the use of the phrenic nerve is accompanied by pulmonary problems in some patients, and thus he is cautious about its use in nerve transfers. Moreover, he cited the work of Chuang and colleagues[1] who pointed out that the phrenic nerve may provide some stabilization of the shoulder but does not provide good shoulder abduction.

According to our experience with treating a large number of patients with BPI, the use of phrenic nerve as a donor nerve became one of our first choices to restore biceps function in multiple cervical nerve avulsions. Biceps muscle strength reached at least Grade 3 in 91.7% of our pa-

Gene Therapy (2006) 13, 106–116

www.nature.com/gt

ORIGINAL ARTICLE

# Enhanced therapeutic efficacy of G207 for the treatment of glioma through Musashi1 promoter retargeting of γ34.5-mediated virulence

R Kanai[1,2], H Tomita[1,2], A Shinoda[1,3], M Takahashi[1,4], S Goldman[5], H Okano[4], T Kawase[2] and T Yazaki[1,2]

[1]Molecular Neurosurgery Laboratory, School of Medicine, Keio University, Tokyo, Japan; [2]Department of Neurosurgery, School of Medicine, Keio University, Tokyo, Japan; [3]Department of Neurosurgery, Chiba Neurosurgical Hospital, Chiba, Japan; [4]Department of Physiology, School of Medicine, Keio University, Tokyo, Japan and [5]Department of Neurology, University of Rochester Medical Center, Rochester, NY 14642, USA

*G207 is a conditionally replicating derivative of herpes simplex virus type1 (HSV-1) engineered with deletions of both ICP34.5 loci and a lacZ insertion disabling the ICP6 gene. G207 exhibits an efficient oncolytic activity* in vitro *and* in vivo, *yet minimal toxicity in normal tissue, and is now in clinical trial for malignant glioma. According to the results of clinical trials, however, although G207 was proved to be safe, the efficacy was not so impressive. Deletion of the ICP34.5 gene coding for virulence made G207 extremely safe, but it markedly reduced the cytotoxicity mediated by HSV-1. To enhance the therapeutic efficacy of G207 without diminishing its safety, we used a defective vector containing Musashi1 promoter/ICP34.5, with G207 as helper virus. P/musashi1 was functional selectively in human glioma cell lines (U87MG, U251, T98G) in this study and dvM345 showed a much higher therapeutic efficacy both in culture and in the* in vivo *glioma model, than G207 alone, without diminishing its favorable toxicity profile. These results suggest that transcriptional regulation of ICP34.5 by P/musashi1 can be used to target HSV-1 virulence toward gliomas while maintaining the desirable neuroattenuated phenotype.*
Gene Therapy (2006) **13**, 106–116. doi:10.1038/sj.gt.3302636; published online 15 September 2005

**Keywords:** *oncolytic herpes vector; G207; glioma; transcriptional control; Musashi1*

## Introduction

G207, a replication-competent HSV-1 vector, possessing deletions in both copies of the ICP34.5 gene and an insertional mutation in the ICP6 gene, has been proven safe through a number of animal experiments and clinical trials.[1–3] G207 exhibits an efficient oncolytic activity in a number of *in vitro* and *in vivo* studies, yet minimal toxicity in normal tissue.[4,5] According to the results of clinical trials, however, it seems that the therapeutic efficacy of G207 was insufficient to treat human gliomas in actual clinical settings. Deletion of the ICP34.5 gene, which is also called the neurovirulence factor and functions by enhancing the viral burst size of infected cells,[6,7] severely attenuated G207 oncolytic activity. In order to enhance therapeutic efficacy, without diminishing its safety, glioma-selective expression of ICP34.5 in oncolytic HSV has been sought.

Musashi1, a neural RNA binding protein, is an evolutionarily well-conserved marker for neural stem cells/progenitor cells.[8–11] Recently, it has been elucidated that Musashi1 is expressed by a variety of tumors, especially malignant gliomas and could be used as a marker for malignant gliomas.[12,13] On the other hand, it was shown that the mouse Musashi1 promoter (P/musashi1) is functional also in the fetal human brain, and neural stem cells can be sorted by fluorescence-activated cell sorting (FACS) on the basis of P/musashi1-driven green fluorescent protein (GFP) expression.[14]

Several strategies were reported to render HSV replication selective for tumor cells: (i) deletion or mutation of viral genes needed for replication in postmitotic cells,[15–17] (ii) deletion of the viral genes responsible for regulating viral progeny production,[18–20] (iii) use of tumor-specific promoters to regulate the expression of essential viral genes,[21,22] (iv) altering the receptor specificity of HSV glycoproteins toward tumor rather than normal tissue[23] and so on. Among these, in order to enhance the efficacy of G207, possibly without damaging its safety, we chose the third strategy in this study.

Firstly, we postulated that P/musashi1 would be functional also in malignant gliomas other than in neural progenitor cells, and could thus be used as a tumor-specific promoter to regulate the expression of essential viral genes specifically in malignant gliomas. Then we reasoned that P/musashi1 transcriptional retargeting of γ34.5 might provide a means to achieve selective virulence for gliomas while retaining attenuated

Correspondence: Dr T Yazaki, Department of Neurosurgery, School of Medicine, Keio University, 35 Shinanomachi, Shinjuku-ku, Tokyo 160-8582, Japan.
E-mail: yazakit@sc.itc.keio.ac.jp
Received 9 February 2005; revised 7 July 2005; accepted 1 August 2005; published online 15 September 2005

virulence for normal tissues. In this study, we used a defective vector containing musashi1 promoter/ICP34.5 with G207 as helper virus. We show that this novel system (dvM345), while still exhibiting the requisite degree of safety, has a significantly higher therapeutic efficacy, than G207 alone both in culture and in an *in vivo* glioma model.

## Results

### *Expression of Musashi1 mRNA in malignant glioma cells*

First, we examined the mRNA expression of *musahi1* in 10 human-derived tumor cell lines – three malignant gliomas (U87MG, U251, T98), a neuroblastoma (SK-N-SH), a lung cancer (A549), a gastric cancer (TMK-1), a colon cancer (HT29), a bladder cancer (KU19-9), a renal cell carcinoma (A498), and a prostate cancer (DU145) – by reverse transcriptase-polymerase chain reaction (RT-PCR) analysis. As shown in Figure 1, all malignant glioma cells examined were Musashi1 mRNA-positive. SK-N-SH was also positive. In contrast, Musashi1 mRNA was not detected in the other cancer cell lines tested this time.

### *Transcriptional activity of P/musashi1 in malignant glioma cells*

To discover whether Musashi1 promoter functions in a tumor-type specific fashion, and evaluate the function, the transcriptional activity of P/musashi1 was assayed with GFP reporter plasmids in several tumor cell lines, including gliomas where Musashi1 mRNA is expressed or A549 and HT29, where Musashi1 mRNA expression was not detected by RT-PCR analysis. B104 where P/musashi1 is not functional (data not shown) was used as a negative control. In each cell line, the fluorescence level with the CMV promoter (B) was higher than that with P/musashi1 (A). However, the ratio of (A) to (B) among the cell lines was significantly higher in glioma cell lines than in the other cell lines tested (Figure 2).

### *Patency of pSRaP/musashi1:γ34.5 in U87MG in culture*

To discover and evaluate the effect of γ34.5 expression by pSRaP/musashi1:γ34.5, pSRaP/musashi1:γ34.5 was transfected into U87MG, U251, A549, HT29, and B104. Mock (phosphate-buffered saline (PBS)) and pHmsi1:GFP were used as controls. After the transfection, G207 was superinfected at a multiplicity of infection (MOI) of approximately 0.01. After 2 days, the resultant viral yield (G207) was counted. The ratio of the viral yield of the cells where pSRaP/musashi1:γ34.5 was transfected and the cells where PBS (mock) was transfected was calculated. As expected, the ratio was extremely high in U87MG (81±3.61) and in U251 (51±9.25), while it was almost 1.0 in A549 (1.13±0.15) and in B104 (1.03±0.15) where P/musashi1 does not work efficiently, confirming that ICP34.5 was efficiently expressed by P/musashi1 in U87 glioma cell lines. (As a control plasmid, pHmsi1:GFP was also used, and the result was almost the same as mock (PBS).) Data represent means and s.d. of triplicate trials (Figure 3).

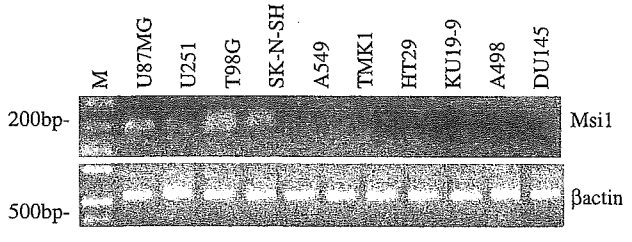


**Figure 1** Expression of Musashi1 gene mRNA in 10 human-derived tumor cell lines. After the isolation of RNA from each cell line, RT-PCR was performed using primer sets for Musashi1 mRNA detection. The PCR products were run on 2% agarose gel and visualized by ethidium bromide staining. A clear band of the expected size (199 bp) appeared in all the glioma cell lines examined and SK-N-SH. On the other hand, no such bands were apparent in cancer cell lines tested here. Primer sets for β-actin were used as a positive control.

### In vitro *cytopathic efficacy*

To analyze the specific cytotoxicity of dvM345, human-derived glioma cell lines in which P/musashi1 works efficiently (U87MG and U251) and the other tumor cell lines in which P/musashi1 does not work efficiently (A549, HT29, and B104) were tested. Cells were infected with dvM345 at an MOI of 0.05, and dvHmsi1:GFP, dvHCRL1, or G207 alone was used as a control. After 18 h postinfection, statistically significant differences were noted between the cytopathic effect of dvM345 and that of control viruses ($P<0.05$, unpaired $t$-test), only in glioma cell lines (Figure 4a and b). On the other hand, in the other tumor cell lines, there was no difference in the cytopathic effect among the viruses used in this study (Figure 4c–e).

### *Growth characteristics of dvM345 in culture*

To see whether the existence of defective vector (dvM345) affects the viral yield of helper virus (G207), single-step growth analysis was performed.

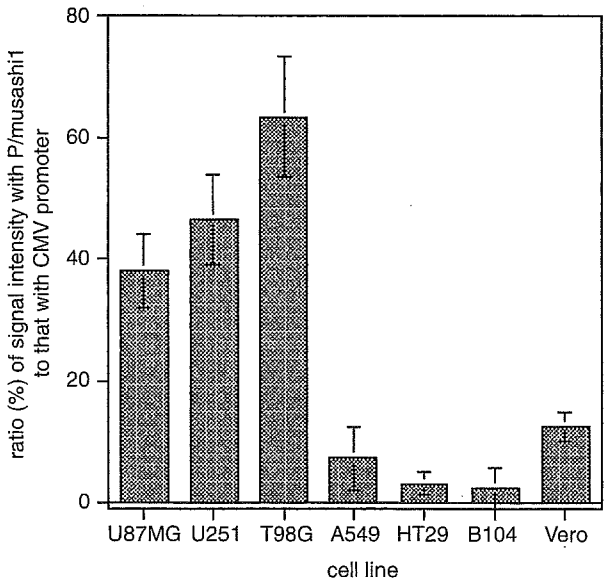


**Figure 2** Transcriptional activity of P/musashi1 in several tumor cell lines. The ratio (%) of the hGFP signal intensity with P/musashi1 to that with the CMV promoter is plotted on the vertical axis. It is significantly higher in glioma cell lines than in the other cell lines tested in this study. The data represents the means±s.d. in triplicate.

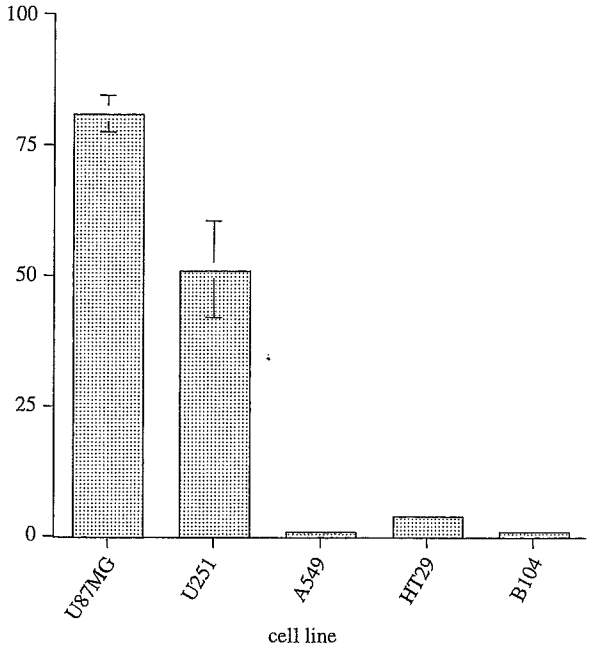


**Figure 3** Patency of pSRaP/musashi1:γ34.5 in U87MG in culture. pSRaP/musashi1:γ34.5 was transfected into U87MG, U251, A549, HT29, and B104. Mock (PBS) and pHmsi1:GFP were used as controls. After the transfection, G207 was superinfected at an MOI of approximately 0.01. After 2 days, the resultant viral yield (G207) was counted. The ratio of the viral yield of the cells where pSRaP/musashi1:γ34.5 was transfected and the cells where PBS (mock) was transfected was calculated. The ratio was extremely high in U87MG (81±3.61) and in U251 (51±9.25), while it was almost 1.0 in A549 (1.13±0.15) and in B104 (1.03±0.15) where P/musashi1 does not work efficiently, confirming that ICP34.5 was efficiently expressed by P/musashi1 in U87 glioma cell lines. Data represent means and s.d. of triplicate trials.

dvHmsi1:GFP and helper virus (G207) alone were used as negative controls. In U87MG, where P/musashi1 works efficiently, the viral yield of G207 in the dvM345 was significantly higher than that in controls ($P<0.05$, unpaired $t$-test) after 12 h postinfection (Figure 5a), while in A549 where P/musashi1 does not work, no difference was observed (Figure 5b).

We next examined this in primary cultures of mouse cortical astrocytes. Monolayers of passage 3 astrocytes were infected with G207, dvM345, or strain F (wild-type HSV-1) at an MOI of 0.1 and followed for 7 days. At 2 days after infection, isolated plaques were visible on strain F-infected cells, but neither on G207-infected cells nor on dvM345-infected cells. By 7 days after infection, total cytopathic effect was observed on strain F-infected cells, whereas no cytopathic effect was observed on G207-infected and on dvM345-infected cells (data not shown).

### *Intraneoplastic inoculation in subcutaneous (s.c.) U87MG tumors*

Xenograft tumors were established in the subcutaneous (s.c.) tissue of the flank of BALB/c (nu/nu) mice, using the U87MG cell line. Once the tumors had reached approximately 6 mm in diameter, $1.0 \times 10^6$ PFU (plaque-forming units) of G207 (group II), dvM345 (group III), or mock extract (group I) was injected intraneoplastically into the flank tumors. From day 6 postinoculation onward, the tumor size of three groups ($n=6$/group) diverged (Figure 6). When the experiment was terminated on day 16 because of the large tumor burden (>24 mm in diameter) in control animals (group I), the difference of the mean tumor growth ratio between group I and group II was statistically significant ($P<0.01$, unpaired $t$-test). More importantly, the difference between group II and group III was also statistically significant ($P<0.01$). The growth ratio of tumors in group II (G207 treatment) on day 16 was 9.94±1.13 (s.e.m.), that in group III (dvM345 treatment) was 1.42±0.71, while that in group I (mock extract) was 21.9±1.37.

All mice, both in the mock infection group and the G207-treated group died because of tumor burden, although mice in the G207-treated group survived longer. In contrast, mice in the dvM345-treated group survived even longer ($P<0.05$ versus G207; Wilcoxon test).

We also employed $2.0 \times 10^6$ PFU in an s.c. tumor model ($n=3$) and obtained similar results (dvM345 showed enhanced efficacy compared with G207).

### *Survival of athymic mice implanted with U87 intracerebral gliomas after treatment with dvM345*

In the survival study using nude mice with the intracerebral (i.c.) U87 tumor model, there was a statistically significant prolongation in the survival of mice treated with dvM345 (group III), compared with survival of mice treated with G207 (group II) ($P<0.01$; Wilcoxon signed rank test) or mock extract (group I) ($n=6$/group) ($P<0.001$; Wilcoxon signed rank test) (Figure 7).

We also employed $1.0 \times 10^6$ PFU in an i.c. tumor model ($n=3$). All mice treated with G207 died within 32 days after tumor implantation. In contrast, one mouse treated with dvM345 survived 80 days after treatment (=90 days after tumor implantation). The other two mice died at day 36 and day 44 after tumor implantation.

### *Histological analysis of viral transduction by X-gal staining in gliomas*

To assess the viral transduction in U87MG i.c. tumors *in vivo*, mice bearing i.c. U87MG tumors were treated, on day 17 postimplantaion, with $5.0 \times 10^5$ PFU of G207 (group II) or dvM345 (group III) and killed on day 5 postinoculation (on day 22 post-tumor implantation). These tumors were stained with X-gal to examine the extent of β-galactosidase expression. Mock-infected tumors showed no β-galactosidase expression (Figure 8a). Although tumors in both group II and group III showed β-galactosidase expression, the extent of expression in group III was remarkably larger than that in group II (Figure 8b and c).

### *Safety evaluation of dvM345 in mice*

To evaluate the safety of dvM345, firstly, three BALB/c mice were tested. For i.c. injection, $5.0 \times 10^6$ PFU was the highest dose technically obtained in this time. All the mice were still alive 3 months after virus inoculation without any noticeable side effects. The sections of their brains, lungs, livers, and kidneys showed no abnormality other than the scar around the needle tract. Secondly,

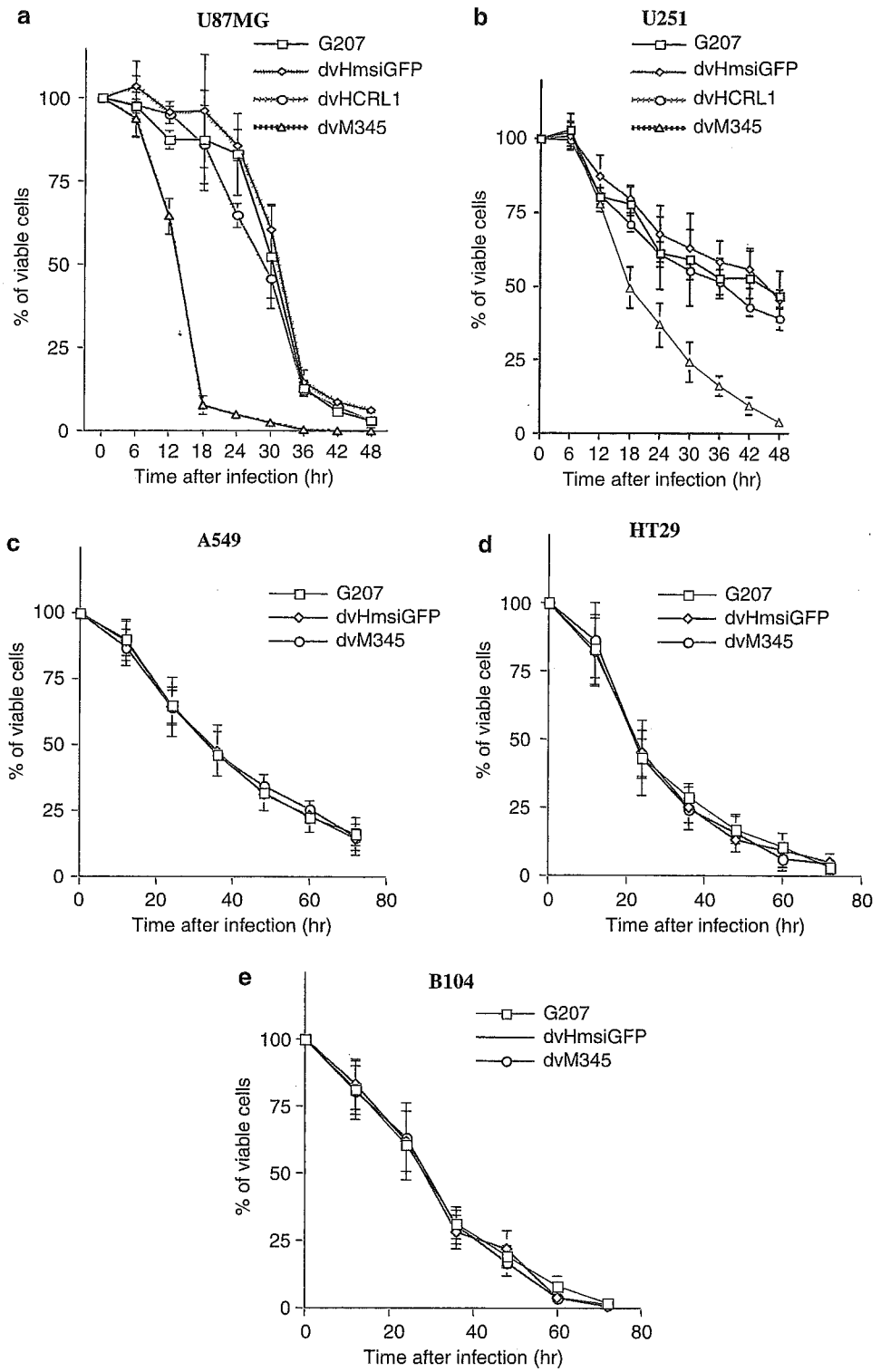


**Figure 4** In vitro cytopathic efficacy of dvM345 on various tumor cell lines: (**a**) U87MG, (**b**) U251, (**c**) A549, (**d**) HT29, and (**e**) B104. As control viruses, dvHmsi1:GFP, dvHCRL1, and G207 alone were used in (**a**) and (**b**). In (**c**)–(**e**), dvHmsi1:GFP and G207 alone were used as controls. Between dvM345 and control viruses, a statistically significant difference in the cytotoxic effect was observed after 18 h postinfection both in (**a**) and (**b**) ($P<0.05$; unpaired $t$-test), while in (**c**)–(**e**) there was no significant difference between dvM345 and control viruses. The data plotted are the means ± s.d. of triplicate trials.

another 10 BALB/c mice were inoculated at the same dose. Every 7 days, until 28 days after the challenge, we assayed brain homogenates for infectious virus by plaque assay. Infectious virus could never be detected thoughout this schedule by plaque assay with X-gal staining or Giemsa's staining. Lastly, persistence of viral DNA in brain tissue (the inoculated site) 4 weeks after the challenge was detected by PCR amplification, using

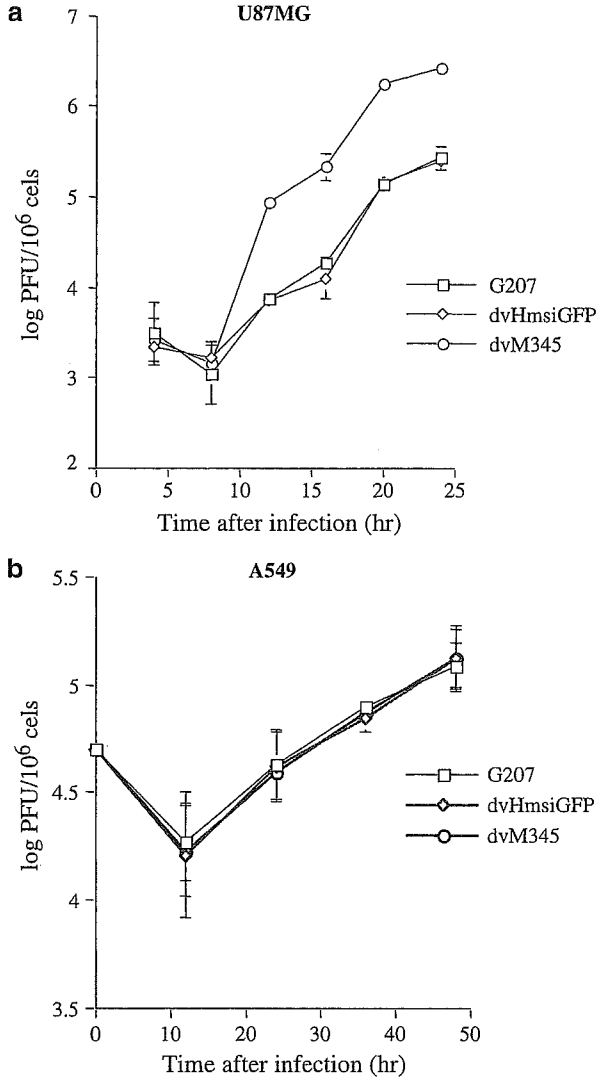


**Figure 5** Single-step viral growth of dvM345 on the U87MG (**a**) and A549 (**b**). The titer of helper virus (G207) was counted every 4 h postinfection. dvHmsi1:GFP and helper virus (G207) alone were used as controls. In U87MG, where P/musashi1 functions efficiently, dvM345 increases the progeny virus production, whereas in A549, where P/musashi1 does not efficiently function, no such effect was seen.

primers from LacZ, which amplify sequences of 300 bp (Figure 9). However, viral DNA was not detected in other tissues tested during this time (spine, lung, liver, spleen, and kidney) (Figure 9).

## Discussion

The malignant glioma, especially glioblastoma multiforme (GBM), is the most common and aggressively invasive form of primary brain tumor in adults.[24] Since GBM tends to extensively infiltrate surrounding normal brain tissue, complete removal of tumor cells is virtually impossible even with the aid of recent improvements in neuroimaging and surgical techniques, necessitating other forms of therapy. Despite major advances in diagnostic procedures, radiation therapy, and chemotherapy, these neoplasms are highly resistant to conventional treatments.[25–27] Consequently, the prognosis for patients has remained poor in the past two decades, and the majority of patients succumb to the disease within 1 year after diagnosis.[28] The absence of an effective treatment and the extremely poor prognosis of this disease necessitate new therapeutic options such as gene therapy.[29–31]

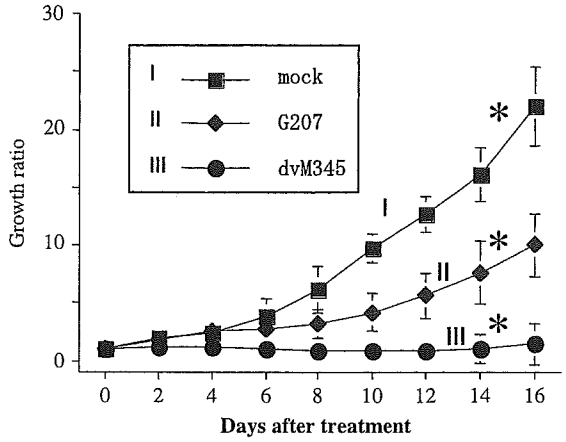


**Figure 6** The intraneoplastic inoculation of G207 (group II) and dvM345 (group III) in s.c. tumor (U87MG)-bearing BALB/c (nu/nu) mice. Mice harboring s.c. U87MG tumors were treated on day 0 with either mock solution (group I), $1.0 \times 10^6$ PFU of G207 (group II), or $1.0 \times 10^6$ PFU of dvM345 (group III) based on helper virus (G207) titer. Data represent mean tumor growth ratio ± s.d.

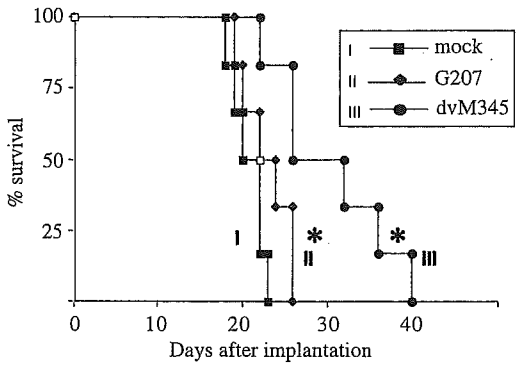


**Figure 7** Extended survival of mice with intracerebral U87MG tumors treated with dvM345. BALB/c nude mice (nu/nu) with intracerebral U87MG tumors (10 days postimplantation) received $5.0 \times 10^5$ PFU of G207 (group II), $5.0 \times 10^5$ PFU of dvM345 (group III), or mock extract (group I). The difference in survival between group III and the other two groups was statistically significant ($P < 0.01$, Wilcoxon signed rank test).

Since replication-defective vectors have to date failed to achieve a high degree of tumor transduction, replication-competent virus vectors appear to be attractive therapeutic agents for cancer.[32–36] Since the first description of a virus that was engineered to replicate selectively in dividing cells 14 years ago,[15] the field of viral therapy for cancer has significantly expanded, and at least 10 different viral species have entered clinical trials.[37] A recent development in cancer gene therapy has revolved around the use of genetically engineered, replication-conditional (oncolytic) viruses to deliver cytotoxic genes to tumor cells as well as destroy them directly via lytic infection.[15,38–41] The use of replication-conditional herpes

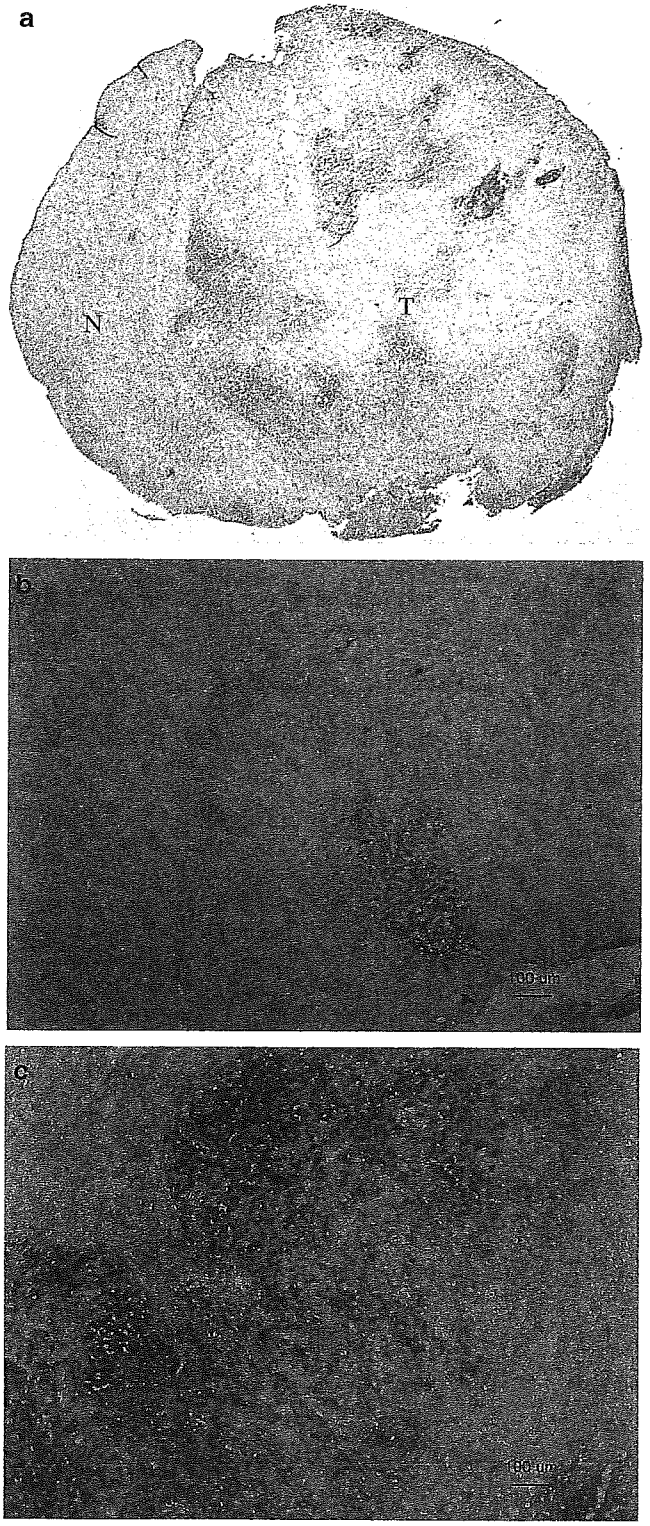


**Figure 8** To assess the viral transduction in U87MG intracerebral tumors *in vivo*, the mice bearing intracerebral U87MG tumors were treated with $5.0 \times 10^5$ PFU of G207 (group II) or dvM345 (group III), and killed on day 5 postinoculation. These tumors were stained with X-gal to examine the extent of β-galactosidase expression. Mock-infected tumors showed no β-galactosidase expression (**a**). Although tumors both in group II (**b**) and group III (**c**) showed β-galactosidase expression, the extent of expression in group III was remarkably larger than that in group II (**b**, **c**). (N: brain; T: tumor).

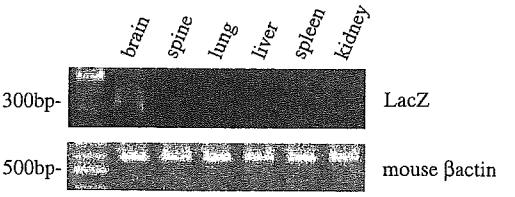


**Figure 9** Persistence of viral DNA in brain tissue (the inoculated site) 4 weeks after the challenge was detected by PCR amplification, using primers from LacZ, which amplify sequences of 300 bp. However, viral DNA was not detected in other tissues tested in this study (spine, lung, liver, spleen, and kidney).

simplex virus type1(HSV-1) mutants appears promising for both of the above-mentioned purposes, since its replication within neoplastic cells should allow enhanced anatomic spread of anticancer effects throughout an inoculated tumor mass and augmentation of this effect by delivery of anticancer genes.[38–48]

Two broad types of replication-conditional HSV mutants in a single gene have been studied to date. The first consists of viral mutants with defects in the function of a viral gene needed for nucleic acid metabolism, such as thymidine kinase, ribonucleotide reductase (RR), or uracyl *N*-glycosylate. The second consists of viral mutants with defects in the function of the γ34.5 gene, which functions as a virulence factor by markedly enhancing the viral burst size of infected cells through suppression of the shutoff of host protein synthesis[6,7,43–45,49,50] and by downmodulating MHC class II cell surface expression.[51] The single-mutant strains have certain inherent limitations, including resistance to ganciclovir for mutants in thymidine kinase, the risk of reversion to wild-type by a single recombination event with wild-type virus, and reduced oncolytic efficacy for γ34.5 mutants, at least in certain tumor cell lines. In an effort to decrease the risk of wild-type recombination, HSV viruses that are multiply mutated have been developed. These include mutants G207 and MGH1, which possess deletions of both copies of γ34.5 and an insertional mutation of RR.[4,52] These double-mutant strains demonstrate markedly reduced neurovirulence upon direct intracranial injection, retain sensitivity to ganciclovir, and show relatively selective replication in tumor cells compared to normal tissues. Such double-mutant HSV strains retain the defective γ34.5 gene, thus demonstrating little virulence toward normal tissues. However, although they clearly demonstrate oncolytic effects against tumor cells, such effects are less than those observed in mutants with intact γ34.5 genes. It could be stated that although the deletion of the γ34.5 gene made G207 extremely safe, it hampered its therapeutic efficacy to an exact. In fact, according to the clinical results reported so far, the efficacy of HSV strains with defective γ34.5 genes in actual clinical settings is not so impressive.[3,33]

Among several strategies to render HSV replication selective to tumor cells, the use of tumor-specific promoters to regulate the expression of essential viral genes is promising.[21,22] Myb34.5, an HSV mutant with deletion in the gene for RR, carries a version of γ34.5 that is under the control of the E2F-responsive cellular B-myb promoter, rather than of its endogenous promoter.[22,53] Compared with HSV mutants with defective γ34.5

expression, Myb34.5 showed enhanced oncolytic efficacy against cycling cells in culture, and showed greater antineoplastic activity in mice with diffuse liver metastases by colon carcinoma.[53]

If, in the context of G207 treatment, the γ34.5 gene were expressed specifically only in glioma cells, the overall therapeutic efficacy should be much higher than when the γ34.5 gene is not expressed. As a candidate for glioma selective promoter, we tested and examined P/musashi1.

Musashi1, an evolutionarily conserved neural RNA-binding protein, has recently been shown to be a versatile marker of human glioma cells.[12,13] Firstly, we checked the mRNA expression of Musashi1 in human glioma cell lines and several of the other cancer cell lines by RT-PCR analysis. We confirmed that Musashi1 mRNA expression is restricted to glioma and neuroblastoma cell lines as far as those tested in this study. This is perfectly consistent with the cases reported earlier.[12,13] Secondly, we investigated the transcriptional activity of P/musashi1, which was originally shown to be functional in neural stem cells of the fetal human brain.[14] We tested the transcriptional activity of P/musashi1 in human glioma cell lines and in several of the other tumor cell lines with a GFP-reporter assay. Our data indicate that the transcriptional activity of P/musashi1 is significantly higher in glioma cell lines than that in the other cancer cell lines investigated. From this result, we postulated that P/musashi1 could be used as a glioma-specific promoter. Thirdly, we constructed a defective virus (dvM345), by reintroducing the γ34.5 gene to G207 under transcriptional control of P/musashi1 in the form of the defective vector. In culture, dvM345 exhibited significantly higher cytopathic efficacy in glioma cell lines than G207 alone or control defective vectors. On the other hand, in the other cancer cell lines tested, the difference between dvM345 and G207 alone was not apparent. The result of the single-step viral growth indicates that in U87MG, the higher cytotoxicity of dvM345 comes from the higher progeny virus (G207)-producing ability of dvM345 in glioma cells where P/musashi1 works efficiently. However, this effect was not observed in A549 where P/musashi1 does not work efficiently, again confirming that the enhanced cytotoxicity of dvM345 is probably tumor-type specific. Next, the *in vivo* therapeutic efficacy of dvM345 was tested using both the s.c. U87 tumor model and the i.c. U87 tumor model in nude mice. In the s.c. tumor model, dvM345 inhibited U87 tumor growth more dramatically than G207 alone. In i.c. U87 tumor model, with a viral PFU as low as $5.0 \times 10^5$, statistically significant increase in survival was seen in the dvM345-treated animals compared with G207-treated group. In both models, the existence of the defective vector (dvM345) enhanced the therapeutic efficacy. Lastly, we examined the safety of dvM345 in mice. Technically, $5.0 \times 10^6$ PFU was the highest titer obtained and tested. The i.c. injection of dvM345 in three BALB/c mice caused no noticeable side effects and all the mice survived 90 days after the challenge. Furthermore, we could not detect infectious virus from as early as 7 days to 28 days after the i.c. inoculation in BALB/c mice. At 28 days after the challenge, also, the persistence of viral DNA in brain tissue (the inoculation site) was detected by PCR amplification, using primers for LacZ. However, it was not the case in tissues other than the inoculation site. Combining these results together, it seems unlikely that neurovirulent recombinants, like hrR3, were generated.[1]

Considering the nature of Musashi1, which is a neural RNA-binding protein preferentially expressed in primitive, undifferentiated CNS cells,[9–11,54] it does not seem likely that its promoter functions in terminally differentiated normal tissue. Our result indicates that P/musashi1 acts in gliomas in addition to the normal fetal neural progenitor cells. While its activity in terminally differentiated normal tissue was not fully examined, the expression level of Musashi1 is much higher in gliomas than in the surrounding normal brain tissues,[12] indicating the glioma selectivity of the present strategy. However, it should be noted that Musashi1 is also expressed in intestinal epithelial stem cells.[55] Thus, the usage of P/musashi1-driven γ34.5 expression in gene therapy might exert some hazardous effects in normal intestinal stem cells and their progenies (normal intestinal mucosa). However, we do not consider that this possibility is likely to be true based on the following reasons. First, the *cis* elements that are involved in the transcriptional activation of Musashi1 in the intestinal stem cells are not likely to be present within P/musashi1 used in our present and previous studies.[14] Based on previous reports, canonical Wnt signaling is likely to play an important role in the Musashi1 expression in the intestinal stem cells and intestinal adenomas[55] as well as in the maintenance of the intestinal stem cells.[55,56] However, the *trans*-activation of P/musashi1-dependent reporter was not induced by the activation of canonical Wnt pathway in the transient transfection assay using the stabilized β-catenin and Tcf-4 expression vectors (S Fukami, T Imai, and Okano, H; unpublished observation). Thus, it is likely that *cis* elements that are present outside of P/musashi1 are involved in the Musashi1-expression in the intestinal stem cells.[57]

In this study, in the context of HSV oncolytic viral therapy, we used a defective vector containing musashi1 promoter/ICP34.5 with G207 as helper virus in order to express ICP34.5 in a glioma-specific fashion and as a result, enhancement of the therapeutic efficacy of G207 was achieved without damaging its safety.

## Materials and methods

### *Cell lines*

Human glioma cell lines (U87MG, U251, and T98G), human neuroblastoma cell line SK-N-SH, six human-derived cancer cell lines (lung cancer (A549), gastric cancer (TMK-1), colon cancer (HT29), bladder cancer (KU19-9), renal cell carcinoma (A498), prostate cancer (DU145)), rat neuroblastoma cell line B104, and African green monkey kidney cells (Vero cells) were obtained from the American Type Culture Collection (Manassas, VA, USA). Human glioma cell lines, SK-N-SH, A549, KU19-9, A498, B104, and Vero cells were cultured in Dulbecco's modified Eagle's medium (DMEM) supplemented with 10% heat-inactivated fetal bovine serum (IFBS). TMK-1 and HT29 were grown in RPMI1640 medium supplemented with 10% IFBS. All cell lines were maintained at 37°C in humidified 5% $CO_2$ with antibiotics (Sigma, St Louis, MO, USA) added to the medium. Passages were usually performed twice a week

with 0.25% trypsin-ethylenediaminetetraacetic acid solution (Sigma).

### *RT-PCR analysis for Musashi1*

The expression of Musashi1 mRNA was analyzed with RT-PCR amplification using an RNA panel of 10 human-derived tumor cell lines (U87MG, U251, T98G, SK-N-SH, A549, TMK-1, HT29, KU19-9, A498, and DU145). RNA extraction and RT-PCR were carried out as previously described.[13]

### *Transcriptional activity of the Mushashi1 promoter*

The transcriptional activity of P/musashi1 in human glioma cell lines (U87MG, U251, and T98G) or other tumor cells (A549, HT29, B104, and Vero cells) was assayed by GFP reporter plasmids, of which the following were used in this study: pm-msi:GFP(truncated),[14] pHCMV:GFP, pHmsi:GFP, and pHCMV.SL amplicon vector. pHCMV.SL amplicon vector was provided by Dr Samuel D Rabkin (Department of Neurosurgery, Georgetown University Medical Center, Washington, DC. USA) and used also as a negative control. pHCMV:GFP was constructed as follows: an hGFP-SV 40 poly(A) fragment was excised by *Sac*II (blunted)/*Sal*I from pm-msi:GFP(truncated) and was inserted at the restriction site for *Hind*III(blunted)/*Sal*I of pHCMV.SL, as hGFP was driven under the CMV promoter. pHmsi1:GFP was constructed as follows: pHCMV.SL was digested by *Spe*I and self-ligated, generating pHSL, which lacks the CMV promotor sequence of pHCMV.SL. Then, P/musashi1-hGFP-SV40 poly(A) expression cassette was excised by *Sal*I from pm-msi1:GFP(truncated) and was inserted into pHSL at the restriction site for *Sal*I, as hGFP was driven under P/musashi1. Thus, both pHCMV:GFP and pHmsi1:GFP have the same sequence other than the promoter sequence for hGFP (both have the HSVa and HSVori sequences of pHCMV.SL in common). Cells were plated in glass dishes at a density of $1.0 \times 10^5$ cells/ml 1 day prior to transfection of the GFP reporter plasmids. Cells were washed with PBS and the medium was replaced with OPTI-MEM (GIBCO BRL) and transfected with Lipofectamine Plus reagent (Life Technologies, Gaithersburg, MD, USA). At 48 h after transfection, cell were washed twice with PBS and then fixed with 4% paraformaldehyde (Nacalai Tesque, Tokyo, Japan). Transcriptional activity of GFP reporter plasmids was assessed by the intensity of the (hGFP) fluorescence of each well, measured with FluorImager 595 (Molecular Dynamics Japan, Tokyo, Japan) and quantified with ImageQuaNT analysis software (Molecular Dynamics Japan, Tokyo, Japan). The ratio (%) of the hGFP signal intensity with P/musashi1 (A) to that with the CMV promoter (B) was compared among the cell lines.

### *pSRa P/musashi1:γ34.5 amplicon plasmid construction*

P/musashi1 was excised by *Hind*III/*Sac*II(blunted) from pm-msi1:GFP(truncated)[14] and was incorporated into a pSRaori4 amplicon plasmid, which was provided by Dr Samuel D Rabkin, at the restriction site for *Hind*III/*Bgl*II, generating pSRaori4:P/musashi1. Plasmid pBGL34.5,[22] which contains the entire γ34.5 coding sequence, was a gift from Peter Pechan (Massachusetts General Hospital, Charlestown, MA, USA). The full-length γ34.5 cDNA was excised as an *Nco*I (blunted)–*Sac*I fragment from pBGL34.5, and was ligated into pKF3 (Takara, Japan) at the restriction site for *Bam*HI (blunted)/*Sac*I, in which the BGHpoly(A) sequence had been incorporated beforehand at the restriction site for *Sac*I/*Pvu*II. The resultant γ34.5-BGHpoly(A) sequence was excised by *Sal*I/*Pvu*II, then incorporated into pSRaori4:P/musashi1, generating the amplicon plasmid pSRaP/musashi1:γ34.5, which has P/musashi1 upstream and BGHpoly(A) sequence downstream of γ34.5 cDNA.

As a preliminary study, to observe the effect of γ34.5 expression by pSRaP/musashi1:γ34.5, pSRaP/musashi1:γ34.5 was transfected into U87MG, U251, A549, HT29, or B104 using Lipofectamine Plus reagent. Mock (PBS) and pHmsi:GFP were used as negative controls, and transfected in exactly the same way as pSRaP/musashi1:ICP34.5. At 2 days after the transfection, G207 was superinfected at a low MOI. At 48 h after the superinfection, cells were harvested and the resultant viral yield was titrated on Vero cells as described elsewhere.[15]

### *Generation of dvM345, a P/musashi1 promoter-driven γ34.5-expressing HSV-1 helper/defective virus vector*

A pSRa P/musashi1:γ34.5 amplicon plasmid was transfected into Vero cells using Lipofectamine Plus reagent. After incubation for about 48 h, the medium was removed; the cells were superinfected with G207 at an MOI of 0.02 and cultured in DMEM with 1% IFBS. Viral stocks were generated according to the method described elsewhere.[44] Titration of G207 helper virus was determined by a plaque-forming assay on Vero cells as described previously.[15] The proportion of defective viral vector within each stock was estimated, based on the cell culture cytotoxicity and the single-step viral growth on U87MG, as described below. The best stock, which showed the highest cytopathic efficacy and viral growth on U87MG, appeared at passage 4. This stock was used thereafter in the *in vitro* and *in vivo* experiments. For estimation of defective particle unit (dpu) of the dvM345, we examined the titer (dpu) of control dvHCRL1 (also passage 4) by the method described previously.[59] The titer of defective virus was $6.8 \times 10^7$ dpu/ml, and the helper virus (G207) titer of the same stock was $1.0 \times 10^9$ PFU/ml. The defective vector:helper virus ratio was 1:14.7.

### *Cell culture cytotoxicity*

We created two control helper/defective viral vectors:dvHmsi1:GFP and dvHCRL1.[59] They were gained by the transfection of pHmsi1:GFP (described above) or pHCRL1 described previously[58,59] into Vero cells, accompanied by superinfection of G207 as the helper virus, following exactly the same procedure in which dvM345 was made. In this case also, we used the stock gained at passage 4. U87MG, U251, A549, HT29, and B104 cells ($1.0 \times 10^6$) were plated in six-well dishes, 24 h before virus infection. Virus infection was performed in 0.5 ml of PBS supplemented with 1% IFBS for 30 min. Cells were infected with dvM345 at an MOI of 0.05 PFU/cell based on the helper virus (G207) titer, while the controls were mock infected with the extract, prepared from mock-infected cells by the same procedure as that used

for the virus inoculum. In the same way, cells were infected with dvHmsi1:GFP or dvHCRL1 at an MOI of 0.05 based on G207 titer. As for glioma cell lines (U87MG and U251), dvHCRL1 was also used as a control virus. The viable cell numbers were determined by the Trypan blue exclusion method every 6 h after infection. All assays were performed in triplicate.

### *Single-step viral growth*

Subconfluent monolayers of U87MG or A549 in six-well dishes were infected at an MOI of 0.05 with dvM345, dvHmsi1:GFP, or helper virus (G207) alone in 0.5 ml of PBS supplemented with 1% IFBS. The count was based on the helper virus (G207) titer. Every 4 h after infection, virus was harvested from the wells and titration of the helper virus (G207) was performed. Plaques were counted and expressed as PFU/ml. Again, experiments were performed in triplicate.

We next examined viral growth in primary cultures of mouse cortical astrocytes. Primary mouse cortical astrocytes were prepared from day 18 Balb/c mouse embryos using a modification[60] of a published procedure.[61] Dissected cerebral hemispheres were dissociated by extrusion through steel mesh and addition of trypsin. Washed and pelleted cells were cultured in DMEM supplemented with 10% IFBS and antibiotics.

Monolayers of passage 3 astrocytes were infected with G207, dvM345, or strain F (wild-type HSV-1) at an MOI of 0.1, and followed for 7 days.

### *Animal studies*

Female athymic BALB/c nude mice (*nu/nu*) (6-week-old) and female BALB/c mice (four-week-old) purchased from Japan SLC (Shizuoka, Japan) were kept in groups of five or fewer, housed in sterile cages, and had free access to autoclaved food and water. All animal procedures were approved by the Laboratory Animal Center (School of Medicine, Keio University, Tokyo, Japan). Regarding the surgical procedures, each mouse was anesthetized with an intraperitoneal 0.25 ml injection of a solution consisting of 84% bacteriostatic saline, 10% sodium pentobarbital (50 mg/ml; Abbott Laboratories, Chicago, IL, USA), and 6% ethyl alcohol. Mice were visited daily to check their viability status.

### *Model 1: s.c. tumor model and intraneoplastic inoculation into the s.c. tumor*

The s.c. tumors were induced by right flank injection of $5.0 \times 10^6$ U87MG cells in 50 $\mu$l. About 10 days after implantation, when the size of s.c. tumors reached 6 mm in diameter, mice were randomly divided into three groups ($n = 6$ per group). Mice were treated intraneoplastically with $1.0 \times 10^6$ PFU of G207 (group II) or dvM345 (group III) suspended in 20 $\mu$l of virus buffer. Mice in group I were treated with 20 $\mu$l of mock-infected extract. The tumors were measured by external caliper measurements within 0.1 mm. Serial tumor volume was obtained by bidimensional diameter measurements and the tumor growth ratio was determined as $0.5(a \times b^2)$day $n/0.5(a \times b^2)$day 0, where $a$ is the longer axis and $b$ is the shorter axis.[4,15,21] Animals were killed when the tumor diameter was greater than 24 mm. Statistical differences in growth ratio were assessed by using an unpaired $t$-test.

### *Model 2: i.c. tumor model and inoculation of the virus*

After mice were anesthetized and immobilized in a stereotactic apparatus (D Kopf Instruments, Tujunga, CA, USA). A linear skin incision was made over the bregma and a 1 mm burr hole was drilled in the skull. U87MG cells $2.5 \times 10^5$ in 3 $\mu$l of serum-free medium were stereotactically injected into the right frontal lobe of nude mice, using a 5 $\mu$l Hamilton syringe (Hamilton Company, Reno, NV, USA). After 10 days, mice were randomly divided into three groups ($n = 6$ per group). Then, $5.0 \times 10^5$ PFU of G207 (group II) or dvM345 (group III), or 3 $\mu$l mock-infected extract (group I) was inoculated stereotactically at the same coordinates, and survival was followed. Statistical significance of the difference in survival was assessed by the Wilcoxon signed rank test. For pathological studies, mice were treated with $5.0 \times 10^5$ PFU of G207 or dvM345, 17 days after implantation, and killed on day 5 post-treatment. After being perfused with 0.5% PFA and 0.5% glutaraldehyde (Nacalai Tesque) in PBS, the brains were removed. The specimens were fixed in 0.5% PFA and 0.5% glutaraldehyde in PBS for 24 h at 4°C. The tumors were then placed in substrate solution containing 5-bromo-4-chloro-3-indolyl-$\beta$-D-galactopyranoside (X-gal, 1 mg/ml; Takara, Kyoto, Japan), 5 mM potassium ferricyanide, 5 mM potassium ferrocyanide, and 2 mM magnesium chloride in PBS for 6 h at 37°C, washed with PBS, and incubated overnight in cold PBS containing 30% sucrose. After being frozen in OCT compound (Miles, Elkhart, IN, USA) in liquid nitrogen, the brains around the needle tract were sectioned on a cryostat. The sections were mounted onto gelatin-coated glass slides. The slides were washed with PBS, stained with X-gal again overnight, and then counterstained with Neutral Red (Fisher Scientific, Pittsburg, PA, USA).

### *Model 3: safety evaluation of dvM345 in mice*

To evaluate the safety of dvM345, firstly, $5.0 \times 10^6$ PFU of dvM345 was injected in the right cerebral hemisphere of three BALB/c mice which were killed 90 days post-inoculation. The brains, lungs, livers, and kidneys were removed, fixed and stained in the same manner stated above.

Secondly, the same dose ($5.0 \times 10^6$ PFU) of dvM345 was injected in the right cerebral hemisphere of another 10 BALB/c mice, and killed on 7, 14, 21, and 28 days postinoculation (two mice per time point) by lethal injection (500 $\mu$l of sodium pentobarbital solution).

Brains were removed, quick-frozen and titration of virus was performed following the method described elsewhere.[1] At 28 days postinoculation, furthermore, the remaining two mice were killed and brain tissues around the right frontal cortex (the inoculation site), spines, lungs, livers, spleens, and kidneys were removed. DNA's extracted from these tissues with DNAzol (Invitrogen) following the manufacturer's instruction were used for PCR analysis as described previously.[1] Briefly, the purified DNA was amplified with either a LacZ primer pair that detects uniquely G207 DNA or a mouse $\beta$-actin primer pair, which was used as an internal control For the mouse $\beta$-actin primer pair, the reactions were 30 cycles at a denaturation temperature of 94°C (30 s/cycle), an annealing temperature of 58°C (30 s/cycle), and an extension temperature of 72°C (1 min/cycle).[62] Their

expected product sizes are 300 bp for LacZ and 550 bp for mouse β-actin. The resultant amplified products were fractionated on a 2% agarose gel, which was then visualized by ethidium bromide staining. The efficiency of cDNA synthesis from each sample was estimated by PCR with the mouse β-actin-specific primers.

## Acknowledgements

We thank Drs Robert L Martuza and Samuel D Rabkin for their valuable scientific support. We are also indebted to Dr Takashi Ohigashi, Yoshihide Otani, and the entire staff of the Department of Neurosurgery, School of Medicine, Keio University for their technical assistance. This work was supported in part by a Grant-in-Aid for Scientific Research from the Ministry of Education, Culture, Sports, Science and Technology, Japan to TY, a Grant-in-Aid for Scientific Research from Japan Society for Promotion of Science, and Keio Gijuku Academic Development Funds to TY.

## References

1 Sundaresan P, Hunter WD, Martuza RL, Rabkin SD. Attenuated, replication-competent Herpes simplex virus type1 mutant G207: safety evaluation in mice. *J Virol* 2000; **74**: 3832–3841.

2 Todo T, Feigenbaum F, Rabkin SD, Lakeman F, Newsome JT, Johnson PA *et al*. Viral shedding and biodistribution of G207, a multimutated, conditionally replicating herpes simplex virus type 1, after intracranial inoculation in *Aortus*. *Mol Ther* 2000; **2**: 588–595.

3 Markert JM, Medlock MD, Rabkin SD, Gillespie GY, Todo T, Hunter WD *et al*. Conditionally replicating herpes simplex virus mutant, G207 for the treatment of malignant glioma: results of a phase I trial. *Gene Therapy* 2000; **7**: 867–874.

4 Mineta T, Rabkin SD, Yazaki T, Hunter WD, Martuza RL. Attenuated multi-mutated herpes simplex virus-1 for the treatment of malignant gliomas. *Nat Med* 1995; **1**: 938–943.

5 Yazaki T, Manz HJ, Rabkin SD, Martuza RL. Treatment of human malignant meningiomas by G207, a replication-competent multimutated herpes simplex virus 1. *Cancer Res* 1995; **1**: 4752–4756.

6 Chou J, Kern ER, Whitley RJ, Roizman B. Mapping of herpes simplex virus-1 neurovirulence to gamma$_1$34.5, a gene nonessential for growth in culture. *Science* 1990; **250**: 1262–1266.

7 Chou J, Roizman B. The $\gamma_1$34.5 gene of herpes simplex virus 1 precludes neuroblastoma cells from triggering total shutoff of protein synthesis characteristic of programmed cell death in neuronal cells. *Proc Natl Acad Sci USA* 1992; **89**: 3266–3270.

8 Nakamura M, Okano H, Blendy JA, Montell C. Musashi1, a neural RNA-binding protein required for *Drospohila* adult external sensory organ development. *Neuron* 1994; **13**: 67–81.

9 Sakakibara S, Imai T, Hamaguchi K, Okabe M, Aruga J, Nakajima K *et al*. Mouse-Musashi-1, a neural RNA-binding protein highly enriched in the mammalian CNS stem cell. *Dev Biol* 1996; **176**: 230–242.

10 Good P, Yoda A, Sakakibara S, Yamamoto A, Imai T, Sawa H *et al*. The human Musashi homolog 1 (MSI1) gene encoding the homologue of Musashi/Nrp-1, a neural RNA-binding protein putatively expressed in CNS stem cells and neural progenitor cells. *Genomics* 1998; **52**: 382–384.

11 Kaneko Y, Sakakibara S, Imai T, Suzuki A, Nakamura Y, Sawamoto K *et al*. Musashi1: an evolutionally conserved marker for CNS progenitor cells including neural stem cells. *Dev Neurosci* 2000; **22**: 139–153.

12 Kanemura Y, Mori K, Sakakibara S, Fujikawa H, Hayashi H, Nakano A *et al*. Musashi1, an evolutionarily conserved neural RNA-binding protein, is a versatile marker of human glioma cells in determining their cellular origin, malignancy, and proliferative activity. *Differentiation* 2001; **68**: 141–152.

13 Toda M, Iizuka Y, Yu W, Imai T, Ikeda E, Yoshida K *et al*. Expression of the neural RNA-binding protein musashi1 in human gliomas. *GLIA* 2001; **34**: 1–7.

14 Keyoung HM, Roy NS, Benraiss A, Louissaint Jr A, Suzuki A, Hashimoto M *et al*. High-yield selection and extraction of two promoter-defined phenotypes of neural stem cells from the fetal human brain. *Nat Biotechnol* 2001; **19**: 843–850.

15 Martuza RL, Malick A, Markert JM, Ruffner KL, Coen DM. Experimental therapy of human glioma by means of a genetically engineered virus mutant. *Science* 1991; **252**: 854–856.

16 Boviatsis EJ, Scharf JM, Chase M, Harrington K, Kowall NW, Breakefield XO *et al*. Antitumor activity and reporter gene transfer into rat brain neoplasms inoculated with herpes simplex virus vectors defective in thymidine kinase or ribonucleotide reductase. *Gene Therapy* 1994; **1**: 323–331.

17 Pyles RB, Warnick RE, Chalk CL, Szanti BE, Parysek LM. A novel multiply-mutated HSV-1 strain for the treatment of human brain tumors. *Hum Gene Ther* 1997; **8**: 533–544.

18 Markert JM, Malick A, Coen DM, Martuza RL. Reduction and elimination of encephalitis in an experimental glioma therapy model with attenuated herpes simplex mutants that retain susceptibility to acyclovir. *Neurosurgery* 1993; **32**: 597–603.

19 Chambers R, Gillespie GY, Soroceanu L, Andreansky S, Chatterjee S, Chou J *et al*. Comparison of genetically engineered herpes simplex viruses for the treatment of brain tumors in a *scid* mouse model of human malignant glioma. *Proc Natl Acad Sci USA* 1995; **92**: 1411–1415.

20 Kesari S, Randazzo BP, Valyi-Nagy T, Huang QS, Brown SM, MacLean AR *et al*. Therapy of experimental human brain tumors using a neuroattenuated herpes simplex virus mutant. *Lab Investig* 1995; **73**: 636–648.

21 Miyatake SI, Tani S, Feigenbaum F, Sundaresan P, Toda H, Narumi O *et al*. Hepatoma-specific antitumor activity of an albumin enhancer/promoter regulated herpes simplex virus *in vivo*. *Gene Therapy* 1999; **6**: 564–572.

22 Chung RY, Saeki Y, Chiocca EA. B-myb promoter retargeting of herpes simplex virus γ34.5 gene-mediated virulence toward tumor and cycling cells. *J Virol* 1999; **73**: 7556–7564.

23 Laquerre S, Anderson DB, Stolz DB, Glorioso JC. Recombinant herpes simplex virus type 1 engineered for targeted binding to erythropoietin receptor-bearing cells. *J Virol* 1998; **72**: 9683–9697.

24 Chen TC, Hinton DR, Apuzzo MLJ. Malignant progression in gliomas. In: Apuzzo MLJ (ed). *Benign Cerebral Gliomas*, Vol. 1. American Association of Neurological Surgeons: Park Ridge, IL, 1995, pp 181–189.

25 Leweke F, Damian MS, Schindler C, Schachenmayr W. Multidrug resistance in glioblastoma: chemosensitivity testing and immunohistochemical demonstration of P-glycoprotein. *Pathol Res Pract* 1998; **194**: 149–155.

26 Shu HK, Kim MM, Chen P, Furman F, Julin CM, Israel MA. The intrinsic radioresistance of glioblastoma-derived cell line is associated with a failure of p53 to induce p21$^{BAX}$ expression. *Proc Natl Acad Sci USA* 1998; **95**: 14453–14458.

27 Osmak M, Vrhovec I, Skrk J. Cisplatin resistant glioblastoma cells may have increased concentration of urokinase plasminogen activator and plasminogen activator inhibitor type 1. *J Neurooncol* 1999; **42**: 95–102.

28 Davis FG, Freels S, Grutsch J, Barlas S, Brem S. Survival rates in patients with primary malignant brain tumors stratified by patient age and tumor histological type: an analysis based on surveillance, epidemiology, and end results (SEER) data, 1973–1991. *J Neurosurg* 1998; **88**: 1–10.

29 Marconi P, Tamura M, Moriuchi S, Krisky DM, Niranjan A, Goins WF *et al.* Connexin 43-enhanced suicide gene therapy using herpesviral vectors. *Mol Ther* 2000; **1**: 71–81.
30 Moriuchi S, Wolfe D, Tamura M, Yoshimine T, Miura F, Cohen JB *et al.* Double suicide gene therapy using a replication defective herpes simplex virus vector reveals reciprocal interference in a malignant glioma model. *Gene Therapy* 2002; **9**: 584–591.
31 Niranjan A, Wolfe D, Tamura M, Soares MK, Krisky DM, Lunsford LD *et al.* Treatment of rat gliosarcoma brain tumors by HSV-based multigene therapy combined with radiosurgery. *Mol Ther* 2003; **8**: 530–542.
32 Khuri FR, Nemunaitis J, Ganly I, Arseneau J, Tannock IF, Romel L *et al.* A controlled trial of intratumoral ONYX-015, a selectively replicating adenovirus, in combination with cisplatin and 5-fluorouracil in patients with recurrent head and neck cancer. *Nat Med* 2000; **6**: 879–885.
33 Rampling R, Cruickshank G, Papanastassiou V, Nicoll J, Hadley D, Brennan D *et al.* Toxicity evaluation of replication-competent herpes simplex virus (ICP34.5 null mutant 1716) in patients with recurrent malignant glioma. *Gene Therapy* 2000; **7**: 859–866.
34 Kirn D. Clinical research results with dl1520 (Onyx-015), a replication-selective adenovirus for the treatment of cancer: What have we learned? *Gene Therapy* 2001; **8**: 89–98.
35 Advani SJ, Weichselbaum RR, Whitley RJ, Roizman B. Friendly fire: redirecting herpes simplex virus-1 for therapeutic applications. *Clin Microbiol Infect* 2002; **8**: 551–563.
36 Nishiyama Y. Herpes simplex virus gene products: the accessories reflect her lifestyle well. *Rev Med Virol* 2004; **14**: 33–46.
37 Kirn D, Martuza RL, Zwiebel J. Replication-selective virotherapy for cancer: bioligical principles, risk management and future directions. *Nat Med* 2001; **7**: 781–787.
38 Chiocca EA. Oncolytic viruses. *Nat Rev Cancer* 2002; **2**: 938–950.
39 Varghese S, Rabkin SD. Oncolytic herpes simplex virus vectors for cancer virotherapy. *Cancer Gene Ther* 2002; **9**: 967–978.
40 Chung RY, Chiocca EA. Gene therapy for tumors of the central nervous system. *Surg Oncol Clin NA* 1998; **7**: 589–602.
41 Boviatsis EJ, Chase M, Wei MX, Tamiya T, Hurford Jr RK, Kowall NW *et al.* Gene transfer into experimental brain tumors mediated by adenovirus, herpes simplex virus, and retrovirus vectors. *Hum Gene Ther* 1994; **5**: 183–191.
42 Moriuchi S, Oligino T, Krisky D, Marconi P, Fink D, Cohen J *et al.* Enhanced tumor cell killing in the presence of ganciclovir by herpes simplex virus type 1 vector-directed coexpression of human tumor necrosis factor-alpha and herpes simplex virus thymidine kinase. *Cancer Res* 1998; **58**: 5731–5737.
43 McKie EA, MacLean AR, Lewis AD, Cruickshank G, Rampling R, Barnett SC *et al.* Selective *in vitro* replication of herpes simplex virus type 1 (HSV-1) ICP34.5 null mutants in primary human CNS tumours – evaluation of a potentially effective clinical therapy. *Br J Cancer* 1996; **74**: 745–752.
44 Papanastassiou V, Rampling R, Fraser M, Petty R, Hadley D, Nicoll J *et al.* The potential for efficacy of the modified (ICP34.5−) herpes simplex virus HSV1716 following intratumoral injection into human malignant glioma: a proof of principle study. *Gene Therapy* 2002; **9**: 398–406.
45 Detta A, Harland J, Hanif I, Brown SM, Cruickshank G. Proliferative activity and *in vitro* replication of HSV1716 in human metastatic brain tumors. *J Gene Med* 2003; **5**: 681–689.
46 Bennett JJ, Adusumilli P, Petrowsky H, Burt BM, Roberts G, Delman KA *et al.* Up-regulation of GADD34 mediates the synergistic anticancer activity of mitomycin C and a $\gamma_1$34.5 deleted oncolytic herpes virus (G207). *FASEB J* 2004; **18**: 1001–1003.
47 Taneja S, MacGregor J, Markus S, Ha S, Mohr I. Enhanced antitumor efficacy of a herpes simplex virus mutant isolated by genetic selection in cancer cells. *Proc Natl Acad Sci USA* 2001; **98**: 8804–8808.
48 Liu BL, Robinson M, Han ZQ, Branston RH, English C, Reay P *et al.* ICP34.5 deleted herpes simplex virus with enhanced oncolytic, immune stimulating, and anti-tumour properties. *Gene Therapy* 2003; **10**: 292–303.
49 Farassati F, Yang AD, Lee PW. Oncogenes in Ras signalling pathway dictate host-cell permissiveness to herpes simplex virus 1. *Nat Cell Biol* 2001; **3**: 745–750.
50 He B, Chou J, Brandimarti R, Mohr I, Gluzman Y, Roizman B. Suppression of the phenotype of $\gamma_1$34.5− herpes simplex virus 1: failure of activated RNA-dependent protein kinase to shut off protein synthesis is associated with a deletion in the domain of the α47 gene. *J Virol* 1997; **71**: 6049–6054.
51 Trgovcich J, Johnson D, Roizman B. Cell surface major histocompatibility complex class II proteins are regulated by the products of the $\gamma_1$34.5 and $U_L$41 genes of herpes simplex virus 1. *J Virol* 2002; **76**: 6974–6986.
52 Kramm CM, Chase M, Herrlinger U, Jacobs A, Pechan PA, Rainov NG *et al.* Therapeutic efficiency and safety of a second-generation replication-conditional HSV1 vector for brain tumor gene therapy. *Hum Gene Ther* 1997; **8**: 2057–2068.
53 Nakamura H, Kasuya H, Mullen JT, Yoon SS, Pawlik TM, Chandrasekhar S *et al.* Regulation of herpes simplex virus $\gamma_1$34.5 expression and oncolysis of diffuse liver metastases by Myb34.5. *J Clin Invest* 2002; **109**: 871–882.
54 Sakakibara S, Okano H. Expression of neural RNA-binding proteins in the postnatal CNS: implications of their roles in neuronal and glial cell development. *J Neurosci* 1997; **17**: 8300–8312.
55 Potten CS, Booth C, Tudor GL, Booth D, Brady G, Hurley P *et al.* Identification of a putative intestinal stem cell and early lineage marker; musashi-1. *Differentiation* 2003; **71**: 28–41.
56 Pinto D, Gregorieff A, Begthel H, Clevers H. Canonical Wnt signals are essential for homeostasis of the intestinal epithelium. *Genes Dev* 2003; **17**: 1709–1713.
57 Giles RH, Vanes JH, Clevers H. Caught up in a Wnt storm: Wnt signaling in cancer. *Biochim Biophys Acta* 2003; **1653**: 1–24.
58 Kaplitt MG *et al.* Expression of a functional foreign gene in adult mammalian brain following *in vivo* transfer via a herpes simplex virus type 1 defective viral vector. *Mol Cell Neurosci* 1991; **2**: 320–330.
59 Yazaki T, Martuza RL, Rabkin SD. Expression of L1 in primary astrocytes via a defective herpes simplex virus vector promotes neurite outgrowth and neural cell migration. *Mol Brain Res* 1996; **43**: 311–320.
60 Asou H, Hirano S, Kohsaka S. Changes in ganglioside composition and morphological features during the development of cultured astrocytes from rat brain. *Neurosci Res* 1989; **6**: 369–375.
61 McCarthy KD, de Vellis J. Preparation of separate astroglial and oligodendroglial cell cultures from rat cerebral tissue. *J Cell Biol* 1980; **85**: 890–902.
62 Morita A, Itoh Y, Toyama T, Fujii H, Nishioji K, Kirishima T *et al.* Activated kupffer cells play an important role in intra-hepatic Th1-associated necro-inflammation in concanavalin A-induced hepatic injury in mice. *Hepatol Res* 2003; **27**: 143–150.

# Pro-Gastrin–Releasing Peptide as a Factor Predicting the Incidence of Brain Metastasis in Patients with Small Cell Lung Carcinoma with Limited Disease Receiving Prophylactic Cranial Irradiation

**Kan Yonemori,** M.D.
**Minako Sumi,** M.D.
**Naoko Fujimoto,** M.D.
**Yoshinori Ito,** M.D.
**Atsushi Imai,** M.D.
**Yoshikazu Kagami,** M.D.
**Hiroshi Ikeda,** M.D.

Division of Radiation Oncology, National Cancer Center Hospital, Tokyo, Japan.

**BACKGROUND.** Prophylactic cranial irradiation (PCI) reduces the incidence of brain metastasis with an effect on overall survival in patients with small cell lung carcinoma (SCLC). In spite of multidisciplinary intensive treatment approaches, many patients still experience brain metastasis. The authors retrospectively analyzed the characteristics of the first failure event due to brain metastasis (FBM) in patients treated with PCI.

**METHODS.** Between January 1990 and April 2004, 71 patients with limited disease SCLC were treated with PCI after completing systemic treatment at the National Cancer Center Hospital (Tokyo, Japan). Univariate and multivariate analyses were used to identify factors related to FBM and survival.

**RESULTS.** The FBM and overall incidence of brain metastasis (OBM) were 16.9 % (12 of 71) and 26.8% (19 of 71), respectively. Median time to progressive disease and median survival were 8.4 months and 21.6 months, respectively. Elevation of pro-gastrin–releasing peptide (Pro GRP) level before PCI was found to be a significant predictive and prognostic factor for FBM, OBM, and survival on multivariate analysis ($P = 0.007$, $P = 0.025$, and $P = 0.009$, respectively).

**CONCLUSIONS.** An elevated Pro GRP level before PCI was found to be significantly related to FBM and survival, and should be considered before PCI is performed. *Cancer* **2005;104:811–6.** © *2005 American Cancer Society.*

**KEYWORDS: prophylactic cranial irradiation, small cell lung carcinoma, limited disease, predictive factor, pro-gastrin–releasing peptide.**

Small cell lung carcinoma (SCLC) accounts for approximately 20% of all lung carcinomas.[1] Although SCLC rapidly develops distant metastasis, it is very sensitive to chemoradiotherapy, unlike non-SCLC. Limited disease SCLC is clinically confined to the hemithorax, and chemoradiotherapy is the standard treatment. In patients with limited disease SCLC, chemotherapy combined with thoracic radiotherapy yields complete remission (CR) rates of 50–85%, with a median survival time of 12–20 months.[2–4] The 5-year survival rate is reported to be 26% for patients who have CR.[4] Because chemoradiotherapy reduces the risk of intrathoracic disease recurrence, distant metastasis in the brain has been the main cause of disease recurrence. Although only 10% of patients have brain metastasis at the time of diagnosis, the cumulative incidence at 2 years is > 50%.[5,6] As many as 73% of patients develop clinically apparent central nervous system metastases before death,[7,8] and even higher rates are documented in autopsy series.[9] The brain is the initial site of disease recurrence in 5–

Address for reprints: Kan Yonemori, M.D., Division of Radiation Oncology, National Cancer Center Hospital, 5-1-1 Tsukiji, Chuo-ku, Tokyo, 104-0045, Japan; Fax: (011) 81-3-3542-3815; E-mail: kyonemor@ncc.go.jp

Received November 1, 2004; revision received March 7, 2005; accepted March 22, 2005.


DOI 10.1002/cncr.21238
Published online 22 June 2005 in Wiley InterScience (www.interscience.wiley.com).

33% of patients, and is the only site of disease recurrence in ≤ 20% of patients.[10,11]

Although several randomized trials of prophylactic cranial irradiation (PCI) have attempted to reduce the risk of brain metastasis and to improve survival, to our knowledge its role in the management of patients with SCLC has remained controversial according to the results of each trial.[12–14]

Recently, the metaanalysis of these trials comparing PCI with no-PCI found that PCI led to a small but significant absolute reduction in mortality (5.4%), and that PCI not only significantly reduced the risk of brain metastasis, but also improved both overall survival (OS) and disease-free survival among patients with SCLC in CR.[15] These results suggest that PCI should be considered as a part of the standard treatment for patients with limited disease SCLC who achieved CR or good partial remission (PR).

Although PCI was performed for patients who achieved CR or good PR as part of the combined treatment that consisted of chemotherapy and thoracic radiotherapy, brain metastasis occurred in 4–24% of the treated patients.[6,12–14] Whole-brain irradiation (WBRT) for brain recurrence was often difficult because these patients had already received PCI to the whole brain. Therefore, we should strictly consider PCI for patients who could achieve a true CR, as assessed with diagnostic imaging. In addition, we should be careful to follow the patients who have a high risk of brain recurrence after PCI.

To our knowledge, there are no previous reports that describe the characteristics of patients with brain metastasis after PCI. In the current study, we analyzed retrospectively predictive factors for brain metastasis in patients with limited disease SCLC treated with PCI.

## MATERIALS AND METHODS

### Patients

A total of 71 patients with limited disease SCLC were treated with PCI after chemoradiotherapy for primary disease between January 1990 and April 2004 at the National Cancer Center Hospital (Tokyo, Japan). Fifty-four patients were male, and the median age was 62 years old (range, 40–75 years).

Histologic or cytologic examination confirmed the diagnosis of SCLC in all patients. Before the initiation of systemic treatment, staging was performed using computed tomography (CT) or magnetic resonance imaging (MRI) scans of the chest, abdomen, and brain, as well as radionuclide bone scanning and bone marrow aspiration and biopsy. Limited disease was defined as being limited to one hemithorax, mediastinal, hilar, or supraclavicular area, which could be encompassed within a reasonable single radiation portal. Patients with pleural effusion found on chest films or CT scan were excluded.

Tumor response was classified in accordance with the World Health Organization (WHO) criteria.[16] After systemic treatment, including thoracic radiotherapy, PCI was administered to patients with CR or good PR according to the results of chest radiography and CT or MRI scans of the head, chest, and abdomen.

### Thoracic Radiotherapy

The majority of patients ($n$ = 55 [77.5%]) received accelerated twice-daily thoracic radiotherapy comprised of 45 gray (Gy) in 1.5-Gy fractions. The remaining patients ($n$ = 16 [22.5%]) received once-daily radiotherapy, 50 Gy in 2-Gy fractions. Radiotherapy was performed 5 days per week, excluding weekends and holidays. Sixty of the 71 patients received concurrent chemoradiotherapy, which began on Day 2 of the first cycle of combination chemotherapy as cisplatin (80 mg/m$^2$, Day 1) plus etoposide (100 mg/m$^2$, Days 1, 2, and 3). The other patients received sequential thoracic radiotherapy after the forth cycle of chemotherapy.

The initial field included the primary tumor volume with a 1.5-cm margin around the mass, the ipsilateral hilum, the entire width of the mediastinum, and the supraclavicular lymph nodes (only if there was tumor involvement).

### Chemotherapy

All patients received cisplatin combination chemotherapy. After concurrent chemoradiotherapy, 34 patients received 3 cycles of cisplatin plus etoposide, 17 patients received CODE therapy (cisplatin at a dose of 25 mg/m$^2$ weekly for 6 weeks; vincristine at a dose of 1 mg/m$^2$ during Weeks 2, 4, and 6; and doxorubicin at a dose of 40 mg/m$^2$ and etoposide at a dose of 80 mg/m$^2$ for 3 days during Weeks 1, 3, and 5), and 9 patients received 3 cycles of cisplatin (60 mg/m$^2$, Day 1) plus irinotecan (60 mg/m$^2$, Days 1, 8, 15). In patients treated with sequential radiotherapy, five patients received four cycles of cisplatin plus etoposide, four patients received four cycles of cisplatin plus irinotecan, and two patients received four cycles of cisplatin containing combination chemotherapy, optimized for each patient.

### Prophylactic Cranial Irradiation

All patients who achieved CR ($n$ =40 [56.3%]) or good PR ($n$ = 31 [43.7%]) were treated with PCI. The median time between the initiation of systemic induction treatment and the initiation of PCI (duration) was 3.7 months (range, 2.6–7.5 months).

The target volume was the entire intracranial site. Individual shaped ports with multileaf collimators